Mineral chemistry of ultramafic massifs in the Southern Uralides orogenic belt (Russia) and the petrogenesis of the Lower Palaeozoic ophiolites of the Uralian Ocean

P. SPADEA[1], A. ZANETTI[2] & R. VANNUCCI[2,3]

[1]*Dipartimento di Georisorse e Territorio, Università di Udine, Via Cotonificio 114, I-33100 Udine, Italy (e-mail: spadea@uniud.it)*

[2]*CNR–Istituto di Geoscienze e Georisorse, Sezione di Pavia, Via Ferrata 1, I-27100 Pavia, Italy*

[3]*Dipartimento di Scienze della Terra, Università di Pavia, Via Ferrata 1, I-27100 Pavia, Italy*

Abstract: Ophiolites of the southern Uralides arc–continent collisional orogen include fertile mantle lherzolites and minor harzburgites in the Nurali and Mindyak massifs located along the Main Uralian Fault suture of the East European craton margin and the Magnitogorsk island arc. We present the first *in situ* analyses of pyroxene from Nurali spinel ± plagioclase-bearing lherzolites and harzburgites and Mindyak spinel lherzolites and harzburgites. Based on the trace element signatures of pyroxene, the Nurali peridotites are divided into: Group 1, consisting of plagioclase-bearing spinel lherzolites with moderately to extremely light rare earth element (LREE)-depleted clinopyroxenes, consistent with ≤8% fractional melting followed by impregnation by incremental to mid-ocean ridge basalt (MORB)-like melts; Group 2, formed by a spinel peridotite with strongly LREE- to middle REE (MREE)-depleted to enriched clinopyroxenes that testify to re-equilibration with large volumes of melt of tholeiitic affinity; Group 3, consisting of amphibole-bearing spinel harzburgites that underwent pervasive percolation of alkali-enriched melts or fluids. Clinopyroxenes from the Mindyak peridotites are strongly depleted and re-equilibrated by reactive porous flow of infiltrating tholeiitic melts. Two alternative petrogenetic models are proposed. In Model 1 the peridotites derive from oceanic lithosphere generated by mid-ocean ridge processes and affected by refertilization via melt percolation. In Model 2 the peridotites were subcontinental lithospheric mantle that experienced deep-seated magmatism and sub-solidus re-equilibration prior to the opening of the Uralian Ocean, and interacted with melts generated in the asthenospheric mantle by extension-related decompression partial melting during the opening of the Uralian Ocean. In both models the final pre-orogenic events are related to the subduction of the Uralian oceanic lithosphere and to mantle wedge processes, notably intrusion of gabbro–diorite at *c.* 400 Ma into the Moho sections.

Mantle peridotite massifs occurring in orogenic belts world-wide represent an exceptional tool to unravel various stages associated with the evolution of a collisional orogen. For example, the peridotite massifs close to the Tertiary suture of the Alps have allowed researchers to document the processes related to the lithospheric break-up (Bodinier *et al.* 1991; Rampone *et al.* 1997) and the formation of Neotethyan oceanic crust (Rampone *et al.* 1996). On the other hand, these mantle rocks maintain records of older subduction events (Zanetti *et al.* 1999) and of a complex multistage evolution under subcontinental conditions (Rampone *et al.* 1993; Rivalenti *et al.* 1995; Mazzucchelli *et al.* 1999).

Ultramafic mantle rocks from the ophiolites of the southern Uralides collisional orogen include fertile mantle lherzolites and minor harzburgites (Savelieva *et al.* 1997, 2002). These peridotites compose a series of massifs located along the Main Uralian Fault, which represents a Late Palaeozoic suture zone between the East European palaeomargin of Baltica and the Devonian island arc (Puchkov 1997a, 1997b; Brown *et al.* 1998).

Extensive alteration of the rocks makes it difficult to decipher the nature of the petrogenetic processes responsible for the evolution of the Main Uralian Fault mantle peridotites and to evaluate the appropriate geodynamic environment of their formation through geochemical modelling of the conventional bulk chemistry. In this study we used *in situ* analyses for a series of geochemically relevant elements of fresh pyroxene from mantle lithologies with the following aims: (1) to

From: DILEK, Y. & ROBINSON P. T. (eds) 2003. *Ophiolites in Earth History*. Geological Society, London, Special Publications, **218**, 567–596. 0305-8719/03/$15

unravel the depletion and enrichment processes that the Uralian peridotites underwent; (2) to evaluate the petrogenetic processes and geological settings recorded by two representative peridotite massifs of the southern Urals, Nurali and Mindyak; (3) to provide geochemical constraints for geodynamic modelling.

The *in situ* pyroxene analyses reported in this paper are the first trace element determinations carried out on fresh mineral phases from the Uralian mantle peridotites.

Geological background

The Uralides are a fold-and-thrust belt that records a Late Palaeozoic arc–continent collisional event along the Eastern European palaeomargin of the Baltica plate (Zonenshain *et al.* 1990; Puchkov 1997a, 1997b; Brown *et al.* 1998). The Main Uralian Fault is a suture zone along which an arc–continent collision took place. It represents the boundary of a continental domain (East European craton) that entered into a subduction zone and collided with an oceanic domain consisting of an intra-oceanic island arc system and dismembered ophiolites. This suture is marked by a mélange zone that can be followed from the Polar Urals segment at 70–66°N to the southern Urals segment at 52–48°N and shows regional trends changing from NE–SW to NNE–SSW toward the south, where the mélange reaches its broadest extension. The main events in the development of the Uralides include development in the Early Palaeozoic of the Eastern European passive margin (Puchkov 1997b) and the generation of a Uralian Ocean recorded by remnants of a Mid-Ordovician basaltic crust (Savelieva & Nesbitt 1996; Savelieva *et al.* 1997). In Silurian–Devonian times, a subduction zone dipping away from the continent generated an intra-oceanic island arc, leading to the closure of the Palaeozoic Uralian Ocean (Savelieva & Nesbitt 1996; Spadea & Scarrow 2000; Savelieva *et al.* 2002; Spadea *et al.* 2002). This island arc complex is preserved in the Polar Urals (Savelieva & Nesbitt 1996; Saveliev *et al.* 1999) and includes a large part of the Tagil zone in the central Urals, where the remnants of mid- and lower arc crust are preserved in the Platinum Belt (Seravkin 1997; Savelieva *et al.* 2002). In the Southern Urals (Fig. 1) the island arc is known as the Magnitogorsk arc, and records the initial subduction in the Early Devonian, *c.* 410 Ma ago, evidenced by the occurrence of boninites in a forearc setting (Spadea *et al.* 1998; Spadea & Scarrow 2000) and the development of a mature, mostly andesitic island arc that followed the formation of these boninites. In Late Devonian to Carboniferous time the Magnitogorsk arc was accreted to the continental margin and an accretionary wedge was generated and emplaced over the subducting slab (Puchkov 1997a, 1997b; Brown *et al.* 1998; Brown & Spadea 1999). The accretionary wedge is composed of Silurian to Mid-Devonian continental slope and platform sedimentary rocks that are overthrust by Late Devonian to Early Carboniferous syncollisional volcanoclastic turbidites derived from the Magnitogorsk arc (Brown *et al.* 1998). These units are flanked to the east by blueschist- and eclogite-facies metamorphic rocks of continental provenance recording a peak metamorphic age of 380–370 Ma (Matte *et al.* 1993; Lennykh *et al.* 1995; Hetzel *et al.* 1998).

The southern Urals ophiolites are different in size and tectonic position. Along the Main Uralian Fault between the accretionary wedge and the Magnitogorsk arc occur several dismembered fragments dominantly made of lenticular or wedge-shaped slabs of mantle ultramafic rocks, several hundred metres to 1 km in size (Fig. 1). These peridotite bodies are composed mainly of lherzolite overlain by mantle restites and ultramafic cumulates representing a crust–mantle transition zone, and intruded by gabbro and diorite (Savelieva 1987; Garuti *et al.* 1997; Savelieva *et al.* 1997, 2002). The Nurali and Mindyak massifs are the best-studied bodies in this group. Fragments of oceanic rocks dispersed as blocks and chips in a mostly serpentinite matrix within the Main Uralian Fault mélange have been interpreted as dismembered pieces of ophiolite sequences. They include serpentinites, ultramafic and mafic cumulates, layered and isotropic gabbros, basalts and diabases, and oceanic sedimentary rocks of Mid-Ordovician age (Gaggero *et al.* 1997; Savelieva *et al.* 1997, 2002; Saveliev *et al.* 1998).

The Kraka ophiolitic massif is a huge body compositionally similar to the Main Uralian Fault ophiolites mentioned above, which is made dominantly of mantle lherzolites, mantle restites and ultramafic cumulates, and blocks of crustal rocks dispersed in a mélange. The Kraka massif is distinct in its structural position in the orogen, in that it occurs as a nappe sheet west of the Main Uralian Fault and thrusts over the Early Palaeozoic sedimentary sequences (Savelieva 1987; Savelieva *et al.* 1997).

In the southernmost Urals east of the Main Uralian Fault, the Kempersay massif shows a complete ophiolite pseudostratigraphy and displays evidence for a complex evolutionary path from oceanic to supra-subduction environment (Melcher *et al.* 1999). It consists of mantle tectonites, mostly harzburgite, overlain by lower cumulates, isotropic gabbro, a well-developed sheeted dyke complex, and basaltic pillow lavas

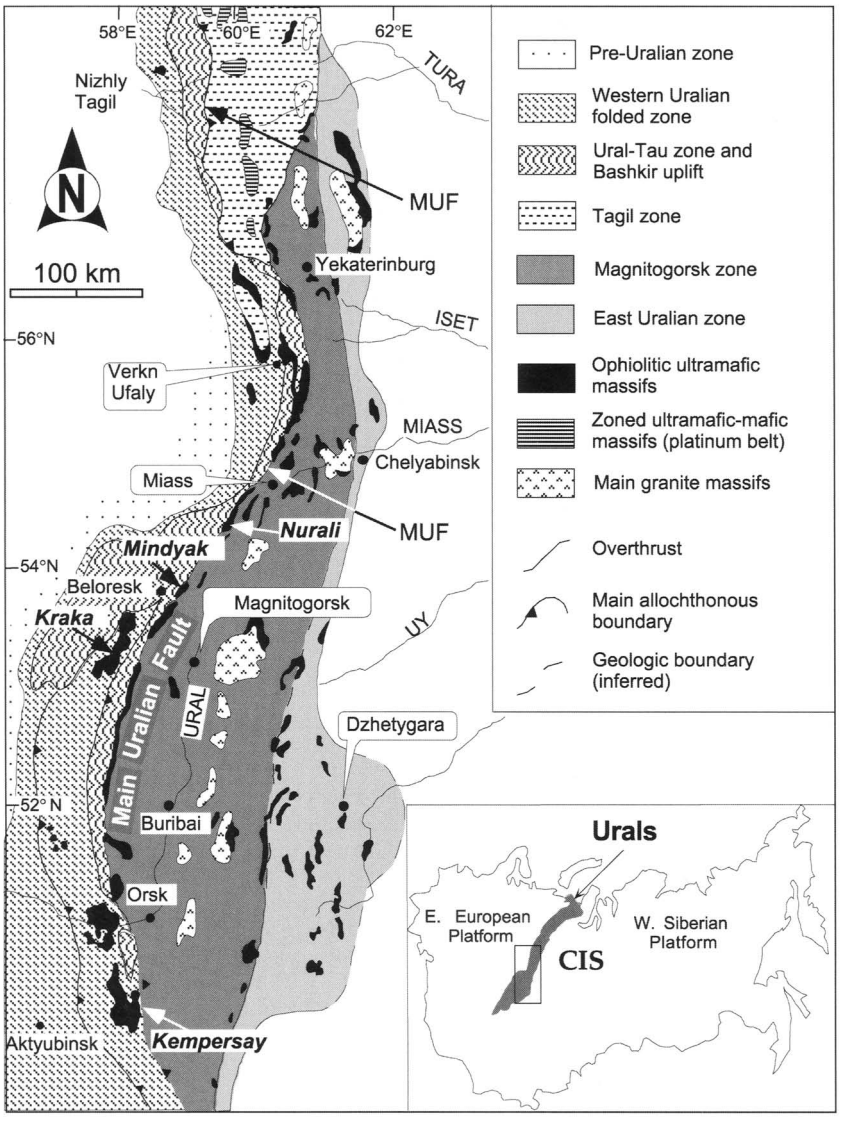

Fig. 1. Geological map of the Southern Urals showing the location of the Main Uralian Fault suture zone with ophiolites, and the main lherzolite massifs of Kraka, Nurali and Mindyak.

capped with Mid-Ordovician phtanites (Ivanov *et al.* 1990; Saveliev & Savelieva 1991; Savelieva & Nesbitt 1996; Savelieva *et al.* 1997, 2002). Radiometric dates reported and discussed by Savelieva *et al.* (2002) have confirmed a Mid-Ordovician age (487 ± 54 Ma) for early generation of the oceanic crust, and much younger, Early Devonian ages (in the 420–387 Ma range), for oceanic closure, obduction and late-stage magmatism.

The geodynamic setting where the southern Urals ophiolites were generated and their role during the complex sequence of events related to the Palaeozoic Uralishes orogeny are still a matter of debate. In fact, even though there is general agreement in identifying the ultramafic and mafic bodies as ophiolitic *sensu lato*, they have been attributed to different geodynamic environments, namely, mid-ocean ridge (Kempersay ophiolite, Savelieva *et al.* 1997, 2002), or continental margin where rapid ascent of mantle diapir caused rifting and was accompanied by low degree of partial melting in the mantle (Kraka and Nurali ophiolite,

Savelieva *et al.* 1997, 2002). The time span from ophiolite protolith generation to emplacement is bracketed between Mid-Ordovician and Early Devonian, and differing pre-orogenic evolutions in a oceanic *sensu lato* setting are inferred from the diversity of internal structure and primary petrological features. On the basis of petrological, geochemical and Nd–Sr isotopic data on the magmatic rocks of the Magnitogorsk arc and those occurring in the Main Uralian Fault mélange, Spadea *et al.* (2002) argued that the Magnitogorsk arc was built on an older (Mid-Ordovician) oceanic crust of mid-ocean ridge type during the closure of the Uralian ocean basin in the Early Devonian. The geodynamic events from sea-floor spreading to oceanic closure are distinct, and the remnants of the Devonian island arc are genetically unrelated to the Main Uralian Fault mantle peridotites. Therefore, the Ordovician oceanic crust should have been trapped during Early Devonian intraoceanic subduction.

Field relations

Nurali massif

The Nurali massif, located about 10 km to the south of Miass, is an ophiolite fragment, mostly peridotitic, elongated NNE–SSW and exposed in an area of about 100 km^2. It is subdivided into a southern body, which is wider and weakly deformed, and a northern body, which is smaller and internally deformed via thrust faulting. The southern body (Figs 2 and 3) shows the mantle section, which consists mostly of lherzolite (about 400 m thick) and grades upward to a crust–mantle transition zone consisting of residual tectonites and ultramafic cumulates. The western margin of this body is marked by a steeply east-dipping contact, emplacing the ophiolite over the Precambrian quartzite and schist of the East European craton. To the east, the crust–mantle transition zone is intruded by diorite and gabbro and is locally affected by a west-dipping, low-angle thrust–fault zone that consists of slabs of volcanic and sedimentary rocks and tectonic breccia. The tectonic breccia includes blocks and chips of various igneous and sedimentary rocks, Silurian to Carboniferous in age, embedded in a serpentinite matrix. Further to the east, Ordovician basalts crop out near the town of Polyakovka, and volcanic rocks (lavas and tuffs mostly of basaltic andesitic composition) of the Magnitogorsk arc crop out along the Irendyk ridge east of Polyakovka.

Along the Nurali ridge, which is the most elevated ridge, reaching about 750 m altitude, the structurally lower part of the mantle section consists mostly of plagioclase-bearing spinel lherzolite and minor spinel lherzolite and spinel harzburgite exposed in a 1.5–1.8 km wide belt (Fig. 3). To the NW it becomes a 0.3–0.5 km wide belt of granular, pyroxene-rich lherzolite. Along the eastern and southeastern slope of the Nurali Ridge the amount of harzburgite and dunite gradually increases, forming a 1.8 km wide belt. To the east of the Nurali ridge, after a large depression overlain by serpentinite, a layered sequence composed of dunite–wehrlite–pyroxenite forms another NNE–SSW ridge of lower altitude.

A detailed structural study by Savelieva (1987) has shown that the plagioclase lherzolites have a nearly horizontal weak foliation, marked by plagioclase and pyroxene, that is associated with an almost horizontal lineation marked by centimetre-sized elongated aggregates of plagioclase and spinel, and less frequently pyroxene. Open folds from 2 m to a few hundred of metres wide, with well-marked hinges plunging 10–30° to the SE, and gently dipping limbs (up to 40°) fold layering. Similar structures continue at depth as observed in drill cores (Savelieva 1987).

In the harzburgite–dunite sequence, layers of orthopyroxene and lineation defined by aggregates of orthopyroxene–spinel–diopside or spinel chains are the main structures. Folding is less pronounced and wider relative to that observed in the plagioclase lherzolites. The foliation of the harzburgite–dunite sequence varies from nearly horizontal in the western part close to the boundary with the plagioclase lherzolites, to dipping to NNE at an increasing angle, to almost vertical at the passage to the dunite–wehrlite–pyroxenite layered sequence. The latter, NE–SW striking and almost vertically dipping, is characterized by folds with axial planes dipping to the east or SE and hinges dipping 60–70° to the east and SE. As a whole, layering of the dunite–wehrlite–pyroxenite sequence is conformable with that of the harzburgite–dunite sequence and discordant with respect to that of the plagioclase-bearing lherzolite.

The dunite–wehrlite–pyroxenite sequence consists of the following lithological types upsection and cropping out from west to east (Savelieva 1987; Pertsev *et al.* 1997): (1) *c.* 10 m of interlayered clinopyroxenite and olivine clinopyroxenite, overlain by fine-grained olivine clinopyroxenite with thin wehrlite and dunite lenses, coarse-grained clinopyroxenite schlieren, and, in the lower part of this interval, up to 10 cm thick chromitite layers (50 m); (2) olivine clinopyroxenite, wehrlite and dunite with layers and lenses of monomineralic diopsidite (Pertsev *et al.* 1997) followed by dunite with chromite interlayers (2–3 mm), and wehrlite and chromitite metre-sized lenses enveloped by serpentinite (140 m); (3) interlayered coarse-

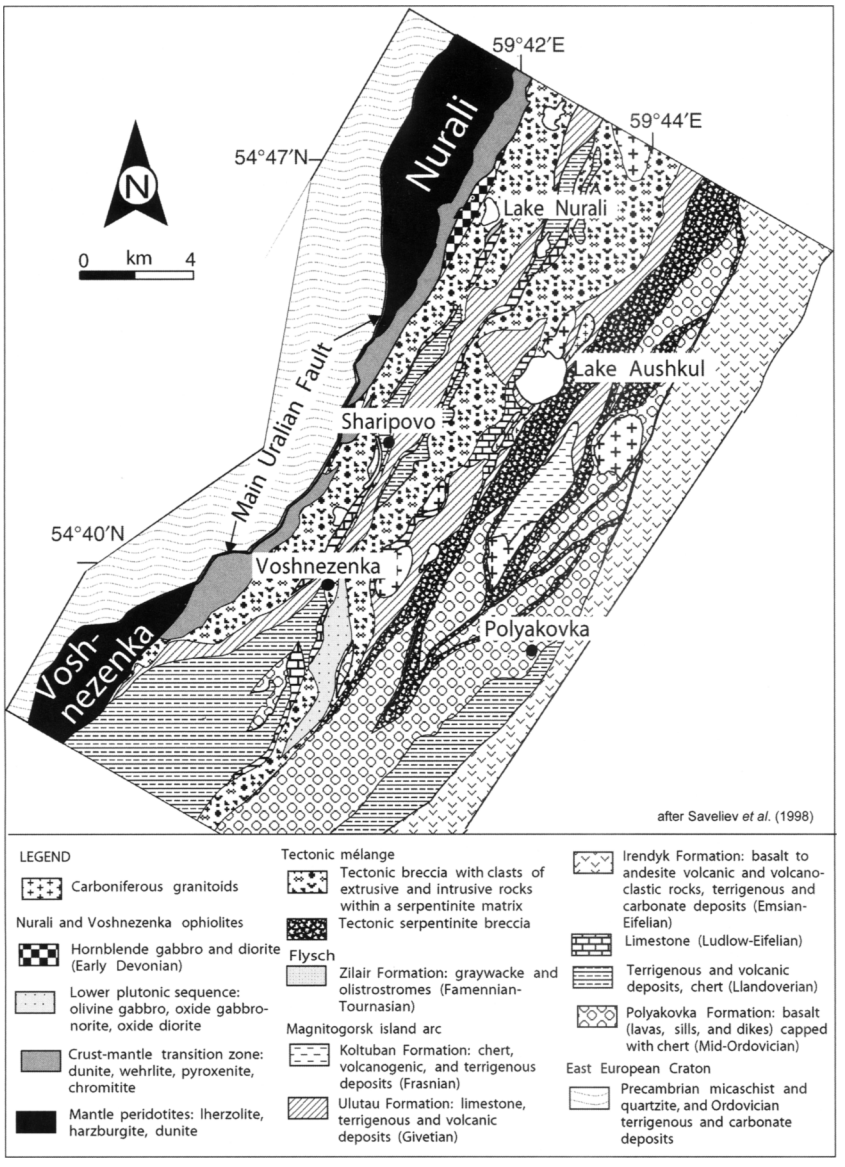

Fig. 2. Geological map of the Nurali–Voshnezenka area (after Saveliev *et al.* 1998). In this area the Main Uralian Fault is marked by a mélange of dismembered ophiolites, monogenetic and polygenetic tectonic breccias, and slices of diverse volcanic and sedimentary sequences, overthrust on Precambrian crystalline schists from the East European craton. The Polyakovka locality, where the Mid-Ordovician oceanic basalts capped with chert are exposed, is shown. The Irendyk Formation represents the upper unit of the Devonian Magnitogorsk arc, which collided in Late Devonian–Early Carboniferous time with the East European continental margin.

grained harzburgite (layers up to 1.5 m thick) and mostly schistose and serpentinized dunite (layers up to 1–2 m thick) with parallel intrusions of banded hornblende ± clinopyroxene oxide gabbro and 1–4 m thick hornblendite concordant with the harzburgite and dunite banding (60 m).

Hornblende gabbro and diorite are intruded into the transition zone with a sharp intrusive contact along its eastern edge. Farther east of this contact the gabbro includes ultramafic xenoliths from the transition zone, and hence providing further evidence of intrusive relationships. A U/Pb age of

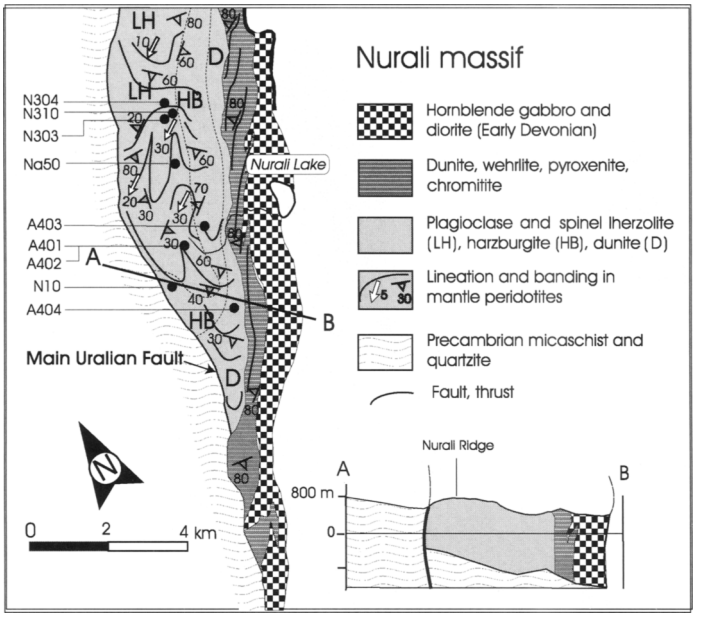

Fig. 3. Geological map and cross-section of the Nurali massif, southern body, The location of the peridotite samples from outcrops (N304, N310, N303, N50, N10, A403) and in boreholes (A403, A401, A402) analysed in this study is shown.

399 Ma for a gabbro–diorite was reported by Pertsev *et al.* (1997).

Mindyak massif

The Mindyak massif, located 20 km to the south of Miass, is a dismembered ophiolite fragment, mostly composed of mantle peridotites, 20 km long by 8 km wide, internally thrust faulted, and elongated NNE–SSW. In the northern and central part (Fig. 4) the peridotites have tectonic boundaries dipping to the east, and locally to the NE as in a rétrocharriage. The western margin of the massif has an overthrust contact with the Precambrian schists of the East European Craton, and/or a polygenetic tectonic breccia with a serpentinite matrix. The eastern margin of the massif is also bounded by a serpentinite tectonic breccia or tectonic slices of the Magnitogorsk arc lavas and volcanoclastic rocks (Irendyk Formation); a flysch of Late Devonian–Carboniferous age (Zilair Formation) overlies the peridotites (Seravkin 1997).

The Mindyak peridotite is mostly composed of spinel and spinel ± plagioclase lherzolites, which become more depleted upwards, while grading into harzburgites and dunites. Upsection, in the eastern part the peridotite body, the crust–mantle transition zone consists of a wehrlite–pyroxenite–dunite association. In the central part of the massif, gabbro and diorite (Denisova 1984) intrude the peridotites and the overlying wehrlite–pyroxenite–dunite sequence.

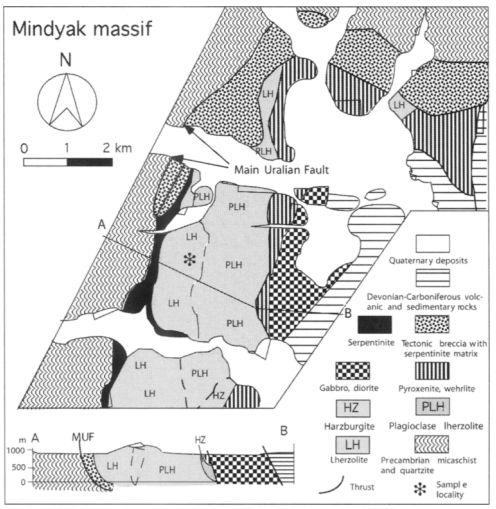

Fig. 4. Geological map and cross-section (redrawn from Denisova 1984) of the central and northern part of the Mindyak massif, and location of the peridotite samples analysed in this study.

The mantle section of the northern part of the Mindyak massif consists of spinel lherzolites grading upsection into harzburgites (analysed in

this study). In the northern part of the massive, near the contact with the crust–mantle transition zone, blocks of metabasites with garnet–pyroxene or garnet–amphibole assemblages are present within a serpentinite breccia (Scarrow *et al.* 2000; Saveliev *et al.* 2001). These rocks have been interpreted as oceanic gabbros that underwent sea-floor alteration and high-pressure metamorphism. They have provided radiometric age constraints for magmatism (an Ordovician minimum age determined on inherited zircon cores) and peak metamorphism (an Early Devonian age of 410 ± 5 Ma determined on zircon populations by U/Pb method, Saveliev *et al.* 2001).

Sample selection for analysis

For the Nurali massif, six samples among the freshest peridotites from the Nurali ridge and three from the harzburgite–dunite sequence have been selected (Fig. 3). Five spinel ± plagioclase lherzolites have been collected from the southern sector of the Nurali ridge (N50, N303, N310, A401 and A402), whereas a spinel lherzolite (H304) sample has been collected from the northern part of the massif. All the samples from the harzburgite–dunite sequence are spinel harzburgites (A403, A404 and N10).

Samples from the Mindyak massif have been collected from the central part (Fig. 4), to document the transition from spinel lherzolites (GS505, GS505-2) to spinel harzburgite (GS505-1, GS505-39).

A synopsis of the distinctive features regarding petrography, mineralogy and geochemistry of the studied samples is presented in Table 1.

Petrography

Nurali peridotites

The spinel ± plagioclase lherzolites from the Nurali ridge are composed of olivine (around 70%), 15–20% orthopyroxene, 5–10% clinopyroxene, 0.5–5% plagioclase and 1–2% spinel. The textures are coarse-granular to porphyroclastic. They are characterized by large (up to 5 mm in size) and deformed (as deduced by the occurrence of kink bands, subgrain boundaries, engulfing of grain edges, bending of elongated orthopyroxene) porphyroclasts of olivine and orthopyroxene, which are embedded in fine-grained (0.2–2 mm) aggregates.

Clinopyroxenes make either interstitial grains or small isodiametric grains included in orthopyroxene. On the basis of the textural relationships, two types of interstitial clinopyroxene (Cpx1 and Cpx2) are recognized. Cpx1 is represented by small (up to 1 mm) anhedral to subhedral (prismatic) clinopyroxenes with large exsolution lamellae (Fig. 5a); this type of clinopyroxene locally shows reactive relationships with plagioclase. Cpx2 is defined by larger (commonly close to 2 mm) anhedral patchy crystals, with no to rare exsolution lamellae, generally poikilitic on small rounded relics of olivine and contains rounded (frequently curved and elongated) plagioclase and secondary, anhedral, orthopyroxene (Fig. 5b). This secondary association of clinopyroxene + plagioclase + orthopyroxene can be interpreted as a coarse-grained symplectite formed by reaction between an interstitial melt and a primary, spinel-facies, mineral assemblage. Similarly, fine-grained aggregates of secondary orthopyroxene and plagi-

Table 1. *Main petrographical and geochemical characteristics of the analysed Nurali and Mindyak mantle peridotites*

Petrography:	Nurali massif				Mindyak massif	
	Spinel plagioclase lherzolite	Spinel plagioclase lherzolite	Spinel lherzolite	Spinel harzburgite	Spinel lherzolite	Spinel harzburgite
Sample:	A401, A402, N303, N310	N50	N304	A403, A404, N10	GS505, GS505-2	GS505-1, GS505-3
Bulk-rock Mg no.	93–91	91	93–91	92	92	91
Bulk-rock La_N/Sm_N	0.16–0.29	0.20	0.60	0.34–1.55	0.31–0.54	1.24–1.45
Bulk-rock La_N/Yb_N	0.03–0.01	0.11	0.14	0.25–1.62	0.69–0.72	0.49–0.74
X_{Cr} spinel	38–44	19–21	35–38	38–51	27–32	31–41
Mg no. spinel	68–55	68–55	68–66	68–62	75–68	66–63
Fo olivine	91–90	91	90	92–91	92–90	91–90
Al_2O_3 opx (wt%)	1.4–4.4	3.2–3.4	2.5–2.6	2.3–2.6	1.4–3.7	2.7–3.0
Al_2O_3 cpx (wt%)	1.4–4.4	3.9–4.4	3.1–3.3	2.6–3.6	2.2–5.3	2.7–3.5
An plagioclase	85–28	–	–	–	–	–

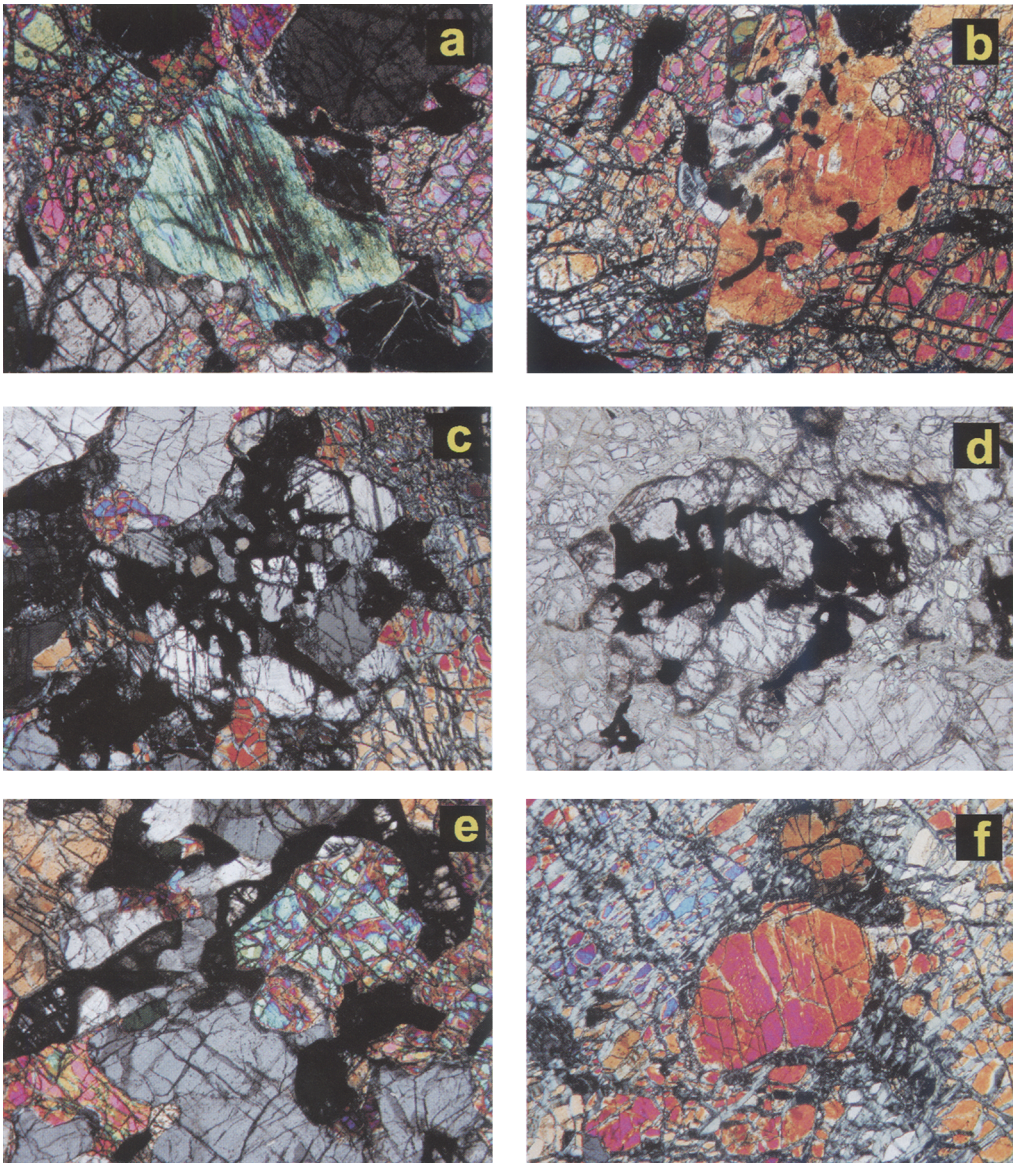

Fig. 5. Petrographic features of spinel–plagioclase and spinel lherzolites from Nurali and Mindyak massifs. Microphotographs with plane-polarized light (**d**) and crossed polars (**a**, **b**, **c**, **e**, **f**); field of view is 3 mm × 2 mm. (**a**) Spinel–plagioclase lherzolite N50: primary clinopyroxene, with turbid core and dense exsolution lamellae (Cpx1). (**b**) Spinel–plagioclase lherzolite N50: symplectite mineral assemblage constituted by Cpx2 (orange–yellow, centre), secondary orthopyroxene (grey, upper left) and plagioclase (black), partially replacing primary olivine as a result of its reaction with percolating melt. (**c**, **d**) Spinel–plagioclase lherzolite A402: largely recrystallized spinel (black) overgrown by a symplectite formed by plagioclase (light grains showing twinning) and orthopyroxene. (**e**) Spinel–plagioclase lherzolite N303: symplectite mineral assemblage formed by secondary orthopyroxene (grey–white) and plagioclase (white indicates preserved; black indicates altered) surrounding and replacing primary olivine. (**f**) Spinel lherzolite GS505-2: clinopyroxene with moderate content of exsolution lamellae (centre) surrounded by strongly serpentinized olivine.

oclase overgrowing primary olivine can be interpreted as cpx-free symplectite (Fig. 5e).

Spinel (brown reddish to dark brown) mostly occurs as skeletal crystals surrounded by and/or intimately interdigitated with relatively large isometric plagioclase (up to 0.6 mm) ± orthopyroxene. Subordinately, subhedral spinel can be found among or within olivine, whereas xenomorphic spinel (0.5–1 mm) is locally placed at the rim of tabular orthopyroxene. The association formed by relics of spinel, plagioclase ± orthopyroxene is present as patches or elongated lenses, 2–3 mm large, placed amongst olivine and orthopyroxene (Fig. 5c and d). Chains of elongated plagioclase–spinel aggregates also occur within pyroxene bands, parallel to the elongation of orthopyroxene porphyryroclasts (e.g. sample N303).

Most of the plagioclase grains are altered and only their primitive habitus can be recognized. Plagioclase makes rounded grains not connected with any pristine spinel, and mainly occurring within fine-grained neoblastic zones. Plagioclase grains are also found: (1) enclosed in secondary clinopyroxene (Cpx2 of cp + opx + plg symplectite); (2) enclosed in reaction zones, where orthopyroxene overgrows olivine (i.e. cpx-free symplectite); (3) along the contact between porphyroclasts. These rounded plagioclase grains commonly have a random distribution, although in some samples they define chains interpretable as pseudo-veins. Small prisms of colourless amphibole are found around chromite grains.

The coarse-grained lherzolites from the northeastern belt consist of 50–60% olivine, up to 30% orthopyroxene and 20% clinopyroxene, and 1–2% spinel, and have coarse-grained (5–10 mm) pyroxenite interlayers. The plagioclase-free lherzolites contain up to 5% diopside and 2% spinel. In the spinel lherzolite N304 (containing 5% clinopyroxene), spinel makes isometric and anhedral grains 0.1–0.2 mm in size, commonly surrounding orthopyroxene, but also placed at the olivine–orthopyroxene boundary and included in olivine. Clinopyroxenes are always strongly exsolved. Also, the orthopyroxenes are exsolved and commonly include poikilitically small, rounded olivine grains.

The harzburgites associated with the lherzolites consist of 80–85% olivine, 10–15% orthopyroxene, 1–2% spinel and minor clinopyroxene (up to 1%). Deformation of olivine and orthopyroxene is similar to that observed in the lherzolites, and recrystallization is moderate. Spinel is present in subhedral grains up to 1 mm in size at contact with orthopyroxene, or included as small grains (0.1–0.2 mm) within both orthopyroxene and olivine. The dunites within the harzburgites consist of coarse-grained olivine (0.6–0.9 mm), with up to 2% chromite and 1% diopside; fine-grained orthopyroxene may be present.

The Nurali peridotites are variously affected by serpentinization. Orthopyroxene is partly transformed to bastite, to a larger extent in harzburgite than in lherzolite. Besides serpentine minerals, magnesite, talc, and carbonate compose the secondary minerals.

Mindyak peridotites

The Mindyak lherzolites (GS505, GS505-2) have protogranular to porphyroclastic textures, with grain size up to 0.9 mm but mostly averaging 0.6–0.2 mm. They consist of 75–80% olivine, 15% orthopyroxene, 5% clinopyroxene, and 1% reddish brown spinel.

Orthopyroxene is generally exsolved and locally bent. Interstitial clinopyroxenes are strongly exsolved in sample GS505, whereas they are not exsolved to slightly exsolved in sample GS505-2. Spinel harzburgites (GS505-1, GS505-3) have porphyroclastic texture with orthopyroxene porphyroclasts up to 2 mm in length. Clinopyroxene is *c.* 1% by volume. However, sample GS505-3 is cut by a pseudo-vein formed by clinopyroxene of 1 mm size. The reddish spinel occurs as isodiametric, subhedral grains (0.1 mm) included in olivine or as anhedral interstitial grains. The studied lherzolite samples are less than 40% modal serpentinized, whereas the harzburgites are between 45 and 90% modal serpentinized, showing extensive bastite formation pseudomorphing orthopyroxene.

Analytical techniques

Bulk-rock XRF analysis was carried out on the PW2400 spectrometer at the Dipartimento di Mineralogia e Petrologia, Padova University (samples N10, N50, N303, N304, N310, A401, A402 and A404), and on the PW1400 spectrometer at the Dipartimento di Georisorse e Territorio, Udine University (samples GS505, GS505-1, GS505-2 and GS505-3). Major elements were measured on lithium borate glass discs prepared with a flux-to-sample ratio of 10:1 to reduce matrix effects. Loss on ignition was determined by the gravimetric method. Bulk-rock trace element analyses (rare earth elements (REE) and V, Cr, Co, Ni, Cu, Zn, Y, Zr and Hf) were carried out by inductively coupled plasma-mass spectrometry (ICP-MS) at the Centro de Instrumentaciòn Cientifica, Granada University. Sample preparation involved digestion of 0.1 g of sample in HNO_3 + HF at high pressure and temperature, evaporation to dryness, and subsequent dissolution in 100 ml of 4 vol.% HNO_3. Measurements were carried out in triplicate with a

PE SCIEX ELAN-5000 spectrometer, with Re and Rh used as internal standards. Precision (2σ) was about ±3 rel.% and ±8 rel.% for concentrations of 50 and 5 ppm, respectively. Minerals were analysed on the WDS Camebax SX50 Cameca at the CNR–Istituto di Geoscienze e Georisorse, Section of Padova. Operating conditions were 15 kV accelerating voltage, 2.2 nA beam current, and synthetic and natural standards were used.

Trace elements in pyroxene were analysed at the CNR–Istituto di Geoscienze e Georisorse, Section of Pavia, by laser-ablation microprobe (LAM)– ICP-MS composed of a double focusing sector field analyser (Finnigan Mat Element) coupled with a Q-switched Nd:YAG laser source (Quantel Brilliant). The fundamental emission of the laser source (1064 nm, in the near-IR region) was converted to 266 nm by two harmonic generators. Helium was used as carrier gas and was mixed with Ar downstream of the ablation cell. Spot diameter was varied in the range 40–60 μm. For quantification BCR2-g glass was used as external standard, with ^{44}Ca as internal standard for clinopyroxene and amphibole and ^{29}Si for orthopyroxene. Detection limits were in the range 100–500 ppb for Sc, Ti and Cr, 10–100 ppb for V, Rb, Sr, Zr, Cs, Ba, Gd and Pb, 1–10 ppb for Y, Nb, La, Ce, Nd, Sm, Eu, Tb, Dy, Er, Yb, Hf and Ta, and usually <1 ppb for Pr, Ho, Tm, Lu, Th and U. Precision and accuracy (both better than 10%) were assessed from repeated analyses of SRN NIST 612 standard. Full details of the analytical parameters and quantification procedures have been given by Tiepolo *et al.* (2003).

Bulk-rock major and trace element chemistry

Bulk-rock major and trace element data for selected Nurali and Mindyak peridotites are presented in Table 2. Relevant major oxides (CaO, Al_2O_3 and MgO) and REE have been selected for chemical characterization and comparison among the peridotites of the two massifs.

Figure 6 shows the Al_2O_3–MgO (a) and CaO–MgO (b) covariation for the selected Nurali and Mindyak peridotites compared with the primitive mantle estimation by Hofmann (1988). The Nurali samples show evidence of linear depletion trends of CaO and Al_2O_3 relative to MgO from plagioclase lherzolite to harzburgite, and a gap of Al_2O_3 abundance, in the 1.5–2.5 wt% interval, from the plagioclase lherzolite and the lherzolite–harzburgite group. The lherzolite and harzburgite samples from Mindyak show ranges of CaO–MgO and Al_2O_3–MgO comparable with those of the spinel harzburgites from Nurali, with distinct trends.

Chondrite-normalized REE patterns are shown in Figure 7a and b (C1 chondrite data after Anders & Grevesse 1989). Nurali plagioclase ± spinel lherzolites are diverse in total REE abundance, with heavy REE ($HREE_N$) up to 2.2, middle REE ($MREE_N$) up to 1.6 and variably depleted light REE (LREE). The La_N/Yb_N ranges between 0.11 for sample N50 (which has the highest total REE content) and 0.02 for sample A401, whereas the La_N/Sm_N is between 0.29 for sample A402 and 0.16 for sample A401. The Nurali N304 spinel lherzolite shows lower HREE content (Yb_N 0.77) than the plagioclase ± spinel lherzolites, but it is less fractionated in the LREE region (La_N/Yb_N and La_N/Sm_N are 0.14 and 0.6, respectively). The Nurali harzburgites are even more markedly impoverished in HREE (Yb_N 0.11–0.29), their patterns being slightly enriched to strongly depleted in LREE (La_N/Yb_N 0.27–1.62; La_N/Sm_N 0.34–1.55).

The overall refractory character shown by the major element composition of the Mindyak peridotites is confirmed by the trace element distribution. Spinel lherzolites have a HREE content ($HREE_N$ 0.4–0.5) significantly lower than that in Nurali lherzolites. On the other hand, their LREE–MREE content is higher than that in the N304 lherzolite and the normalized patterns are flat (La_N/Yb_N 0.31–0.54; La_N/Sm_N 0.57–0.79). Harzburgites show a distinctive MREE–HREE depletion (0.1–0.3 times C1), but the LREE content is similar to or even higher than that in lherzolites. As a consequence, they show concave-downward patterns similar to that of the Nurali N404 harzburgite with La_N/Sm_N of *c.* 2 and La_N/Yb_N of 1.24–1.45.

Major element mineral chemistry

Olivine has forsteritic composition and shows no significant variation within samples. The Fo range is large in the olivine from the Nurali peridotites (Fig. 8c), in which the highest Mg content is shown by olivine from spinel harzburgite A403 (mean Fo 92.4), whereas the lowest is shown by olivine from plagioclase-bearing spinel lherzolite N303 (mean Fo 89.8).

Olivine from the Mindyak peridotites has Fo in the range of 90.5–91.3 (Fig. 8c). The NiO content is moderate (0.10–0.50 wt%).

Clinopyroxene is chromium diopside in the analysed peridotites. Unlike olivine, the clinopyroxenes from some samples (e.g. spinel lherzolite GS505) show significant compositional heterogeneity, in particular in the Al, Cr, Na and Ca contents. The Mg number value (expressed as 100 $Mg/(Mg + Fe^{2+}_T)$) is significantly correlated with the Fo content of the olivine. As a whole, the

Table 2. *Bulk-rock major (XRF data) and trace element (ICP-MS data) composition of Nurali and Mindyak massif mantle peridotites*

	Nurali massif						
Sample:	A401	N303	N50	A402	N310	N304	A403
Rock type:	Plagioclase spinel lherzolite	Plagioclase spinel lherzolite	Plagioclase spinel lherzolite	Plagioclase spinel lherzolite	Plagioclase spinel lherzolite	Spinel lherzolite	Spinel harzburgite
wt%							
SiO_2	44.08	44.14	44.45	44.72	45.84	44.20	43.22
TiO_2	0.04	0.05	0.09	0.03	0.06	0.03	0.03
Al_2O_3	2.50	3.14	2.40	2.71	3.44	1.34	0.82
Fe_2O_3	8.77	8.98	9.10	8.74	8.42	9.43	7.97
MnO	0.13	0.13	0.13	0.13	0.13	0.14	0.11
MgO	42.44	40.63	41.60	41.30	39.08	42.97	47.18
CaO	1.62	2.85	2.56	2.57	3.40	2.04	0.72
Na_2O	0.17	0.23	0.07	0.17	0.30	0.05	0.05
K_2O	0.02	0.03	0.01	0.01	0.03	0.01	0.01
P_2O_5	0.00	0.00	0.00	0.00	0.00	0.00	0.01
Total	99.77	100.18	100.41	100.38	100.70	100.21	100.12
LOI	6.55	4.13	6.49	6.48	3.11	4.89	10.8
Mg no.	0.9055	0.8996	0.9005	0.9035	0.9019	0.9002	0.9214
ppm							
V	37.48	54.69	56.75	47.73	62.41	58.94	26.94
Cr	1698	1648	1657	1867	1982	2090	2189
Co	100.9	100.3	101.5	101.3	96.25	97.58	100.4
Ni	2050	1970	1946	1929	1847	1938	2199
Cu	10.81	27.84	29.81	5.59	12.83	4.85	6.47
Zn	45.38	38.35	36.89	46.33	43.09	45.26	50.31
Y	1.026	1.731	2.073	1.411	2.209	0.699	0.332
Zr	0.141	0.38	2.285	0.127	0.273	0.188	0.253
Hf	0.024	0.049	0.119	0.024	0.05	0.023	0.022
La	0.008	0.019	0.043	0.022	0.022	0.025	0.017
Ce	0.023	0.063	0.181	0.072	0.074	0.075	0.051
Pr	0.004	0.012	0.038	0.015	0.016	0.008	0.01
Nd	0.032	0.125	0.296	0.094	0.096	0.052	0.07
Sm	0.031	0.066	0.136	0.047	0.067	0.026	0.031
Eu	0.018	0.039	0.066	0.023	0.041	0.01	0.013
Gd	0.09	0.176	0.278	0.116	0.208	0.062	0.056
Tb	0.019	0.036	0.053	0.027	0.046	0.014	0.01
Dy	0.166	0.312	0.407	0.226	0.379	0.112	0.071

(*continued overleaf*)

Table 2. (*continued*)

	Nurali massif						
Sample:	A401	N303	N50	A402	N310	N304	A403
Rock type:	Plagioclase spinel lherzolite	Plagioclase spinel lherzolite	Plagioclase spinel lherzolite	Plagioclase spinel lherzolite	Plagioclase spinel lherzolite	Spinel lherzolite	Spinel harzburgite
	0.044	0.077	0.092	0.062	0.096	0.03	0.016
Ho							
Er	0.15	0.237	0.263	0.198	0.301	0.106	0.052
Tm	0.026	0.04	0.043	0.032	0.052	0.017	0.007
Yb	0.175	0.245	0.262	0.2	0.325	0.125	0.047
Lu	0.029	0.043	0.046	0.037	0.054	0.021	0.008
Tm	0.026	0.04	0.043	0.032	0.052	0.017	0.007
Yb	0.175	0.245	0.262	0.2	0.325	0.125	0.047
Lu	0.029	0.043	0.046	0.037	0.054	0.021	0.008
La_N/Sm_N	0.16	0.18	0.20	0.29	0.21	0.60	0.34
Sm_N/Yb_N	0.20	0.30	0.57	0.26	0.23	0.23	0.73
La_N/Yb_N	0.03	0.05	0.11	0.08	0.05	0.14	0.25

	Nurali massif		Mindyak massif			
Sample:	A404	N10	GS505	GS505-2	GS505-3	GS505-1
Rock type:	Spinel harzburgite	Spinel harzburgite	Spinel lherzolite	Spinel lherzolite	Spinel harzburgite	Spinel harzburgite
wt%						
SiO_2	42.25	43.89	43.66	44.37	42.50	44.00
TiO_2	0.01	0.02	0.03	0.03	0.03	0.02
Al_2O_3	0.70	1.11	1.23	1.34	0.73	0.99
Fe_2O_3	8.53	8.66	8.44	8.39	9.47	9.14
MnO	0.12	0.12	0.16	0.13	0.14	0.14
MgO	48.08	45.54	45.32	44.28	46.58	44.31
CaO	0.35	0.70	0.87	0.97	0.18	1.10
Na_2O	0.04	0.04	0.01	<0.01	<0.01	<0.010
K_2O	0.01	0.01	0.00	<0.01	<0.01	0.00
P_2O_5	0.00	0.00	0.02	0.01	0.01	0.01
Total	100.09	100.09	99.77	99.52	99.64	99.71
LOI	10.11	7.00	9.53	8.87	11.56	8.14
Mg-no.	0.9178	0.9124	0.9140	0.9127	0.91	0.9057

ppm						
V	18.61	22.95	34.0	39.0	21.5	28.0
Cr	2236	1907	2086	2547	1891	2070
Co	107.2	108.4	114	124	122	129
Ni	2218	2196	2340	2374	2511	2316
Cu	5.69	6.03	40.8	43.4	43.9	46.9
Zn	40.36	51.4	0.84	1.00	0.66	0.81
Y	0.08	0.239	0.547	0.546	0.273	0.214
Zr	0.604	0.228	1.421	0.831	1.014	1.026
Hf	0.022	0.013	0.045	0.028	0.035	0.031
La	0.042	0.018	0.053	0.034	0.075	0.063
Ce	0.08	0.053	0.134	0.085	0.152	0.141
Pr	0.012	0.008	0.023	0.017	0.022	0.019
Nd	0.057	0.043	0.122	0.088	0.098	0.076
Sm	0.017	0.017	0.042	0.042	0.024	0.019
Eu	0.006	0.008	0.016	0.017	0.007	0.004
Gd	0.019	0.029	0.059	0.063	0.025	0.027
Tb	0.003	0.005	0.011	0.012	0.004	0.005
Dy	0.02	0.043	0.082	0.094	0.038	0.036
Ho	0.004	0.011	0.021	0.021	0.01	0.007
Er	0.014	0.035	0.069	0.067	0.029	0.02
Tm	0.003	0.006	0.011	0.011	0.004	0.004
Yb	0.018	0.047	0.068	0.075	0.042	0.03
Lu	0.004	0.009	0.011	0.012	0.008	0.005
La_N/Sm_N	1.55	0.66	0.54	0.31	1.24	1.45
Sm_N/Yb_N	1.04	0.40	0.78	0.49	1.54	1.81
La_N/Yb_N	1.62	0.27	0.72	0.69	0.49	0.74

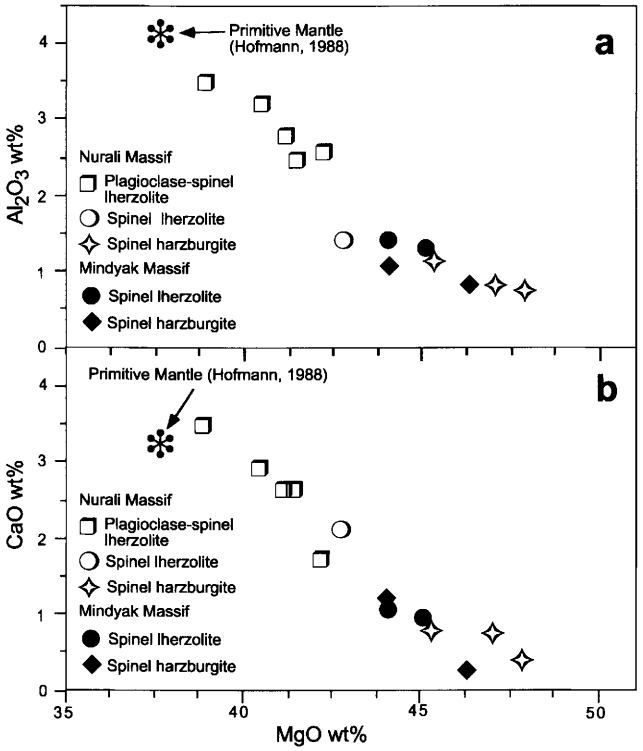

Fig. 6. Variation diagrams of Al_2O_3 (**a**) and CaO (**b**) vs. MgO for Nurali and Mindyak representative peridotite samples selected for the chemical analysis of mineral phases.

Nurali and Mindyak clinopyroxenes show low to moderate Na_2O content (0.3–0.7 wt% in the Mindyak, and 0.2–0.6 wt% in the Nurali peridotites; Fig. 8a), and low TiO_2 (0.09–0.25 wt% in the Mindyak, and 0.03–0.56 wt% in the Nurali peridotites) and Al_2O_3 (3.1–4.4 wt% in the Mindyak, and 2.6–4.1 wt% in the Nurali peridotites; Fig. 8b) contents. Conversely, the Cr_2O_3 content is consistently high (1.1–1.35 wt% in the Mindyak, and 0.8–1.2 wt% in the Nurali peridotites; Fig. 8a). As shown in Figure 8a and b, these compositional features are typical of clinopyroxenes from depleted peridotites, namely, peridotites that have experienced significant episodes of melt extraction (e.g. abyssal peridotites (Johnson *et al.* 1990; Johnson & Dick 1992), and peridotites from extensional environments, such as the Internal Ligurides Unit in the Northern Apennines (Rampone *et al.* 1996) and supra-subduction environments (Bonatti & Michael 1989)).

Orthopyroxenes have enstatite composition with moderately variable Al content (Fig. 8d). In some samples from the Mindyak and Nurali peridotites, orthopyroxenes show extremely variable CaO content (e.g. in spinel harzburgite GS505-3 the CaO varies from 0.77 to 2.44 wt%). The highest CaO content is commonly associated with slightly higher Al_2O_3 and lower MgO and FeO contents, but the Mg number values remain constant. On the other hand, the orthopyroxene with low CaO is statistically dominant. Similar CaO variations have been documented in the peridotites from the Internal Ligurides units (Rampone *et al.* 1996) and interpreted as the result of different T of equilibration. However, the local concentration of exsolved (cryptic) clinopyroxene lamellae cannot be disregarded in explaining the occurrence of the CaO-rich domains. The mean Mg number values are 89.8–92.5 in the Nurali orthopyroxenes, and 90.8–91.4 in the Mindyak orthopyroxenes. These values are roughly correlated with the Fo of the associated olivine, and closely correlated with the Mg number values of the clinopyroxenes, thus suggesting a temperature dependence of the observed Mg–Fe partitioning. Consistently with the clinopyroxenes, the Cr_2O_3 content of orthopyroxene is high (0.36–0.80 wt%), whereas the Al_2O_3 content is rather low (2.3–3.6 wt%).

Spinel is mostly characterized by relatively high Cr (Cr_2O_3 is 26.6–32.5 wt% in Mindyak perido-

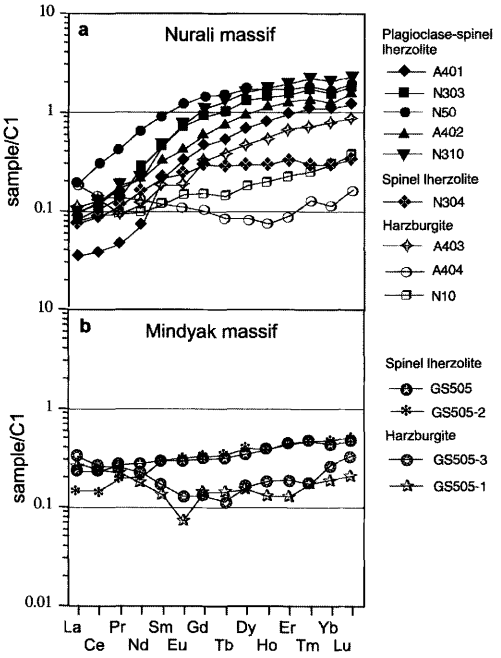

Fig. 7. Chondrite-normalized REE patterns for the Nurali (**a**) and Mindyak (**b**) peridotites. Normalization values after Anders & Grevesse (1989).

tites and 27.6–34.5 wt% in Nurali peridotites) and low Al (Al_2O_3 is 33.6–41.6 wt% in Mindyak peridotites and 27.6–34.5 wt% in Nurali peridotites), with the significant exception of the spinel in the plagioclase ± spinel lherzolite N50, which is more enriched in Al (Al_2O_3 47.5 wt%; Cr_2O_3 17.7 wt%). Most spinel compositions plot in the 'depleted area' of the field defined in the X_{Cr} (expressed as molar 100 × Cr/(Cr + Al)) vs. Mg number (expressed as molar 100 × Mg/(Mg + Fe^{2+})) diagram (not shown) for abyssal peridotites from the North Atlantic (Bonatti *et al.* 1993, and reference therein). The spinel from sample N50 is close to the field of fertile subcontinental peridotites (e.g. External Ligurides in the Northern Apennines; Rampone *et al.* 1993). It is noteworthy that the spinels from both Nurali and Mindyak peridotites plot within the olivine–spinel mantle array defined by Arai (1987) in the X_{Cr} vs. Fo plot (Fig. 8c). Nevertheless, in the Cr-rich samples, the X_{Cr} increases with a decrease of Fo. This correlation is not consistent with the variations induced by different degrees of partial melting and suggests that other processes, such as sub-solidus re-equilibration under plagioclase-facies conditions and/or metasomatism affect spinel compositions.

Plagioclase has been analysed in the N303, N310 and A402 lherzolites. It shows a large variability in anorthite content, with An in the range of 28–82 (N303), 54–78 (N310) and 43–85 (A402) (Fig. 9). This large variation of An is unusual in plagioclase peridotites. As shown by the Ab–An–Or diagrams of Figure 9, for example, plagioclases with different microstructural relations in peridotites from the Internal Ligurides show homogeneous Ca-rich composition (An 91–94). On the other hand, An-poor plagioclase (An down to 46) has been found in granoblastic coronas around spinel from Zabargad peridotites, which have been interpreted as a result of sub-solidus recrystallization at the transition from spinel- to plagioclase-facies conditions (Piccardo *et al.* 1988). It is noteworthy that the plagioclase from melt-impregnated peridotites from Zabargad has An in the range of 80–85, which is very similar to the most Ca-rich composition of the Nurali plagioclase.

Trace element mineral chemistry

Clinopyroxene

Nurali peridotites. The trace element composition of clinopyroxenes from the Nurali peridotites (Table 3) is characterized by a large variability. On the basis of the geochemical affinity, three groups can be tentatively recognized and will hereafter be called Nurali Groups 1–3.

Nurali Group 1 consists of the clinopyroxenes from the plagioclase ± spinel lherzolites (N50, N303, N310 and A402), which show C1-normalized patterns (Fig. 10a) that are strongly to moderately LREE depleted (Ce_N/Yb_N 0.002–0.2) and nearly flat in the HREE region (Yb_N 8.9–15). The LREE depletion is accompanied by low to very low amounts of the highly incompatible elements (Sr 0.09–2 ppm; Zr 0.42–30 ppm; Nb, Ta U and Th are nearly always below the analytical detection limits). The C1-normalized patterns are also characterized by negative Sr and Ti anomalies. The most LREE-depleted samples show also negative Zr and Hf anomalies, whereas these elements are interpolated between the adjacent REE in the N50 clinopyroxenes. The REE distribution of the N50 clinopyroxenes is similar to that shown by the clinopyroxenes from fertile lherzolites (e.g. Zabargad peridotites, Piccardo *et al.* 1993), but it displays some distinctive features, such as larger LREE depletion and large negative Sr anomaly. These latter characteristics are more typical of clinopyroxenes from peridotites that underwent either melt extraction, or melt percolation at low *P* (plagioclase-facies conditions) (e.g. Lanzo peridotites, Bodinier *et al.* 1991; Bracco peridotites, Rampone *et al.* 1997). An extremely LILE-depleted trace element signature has been

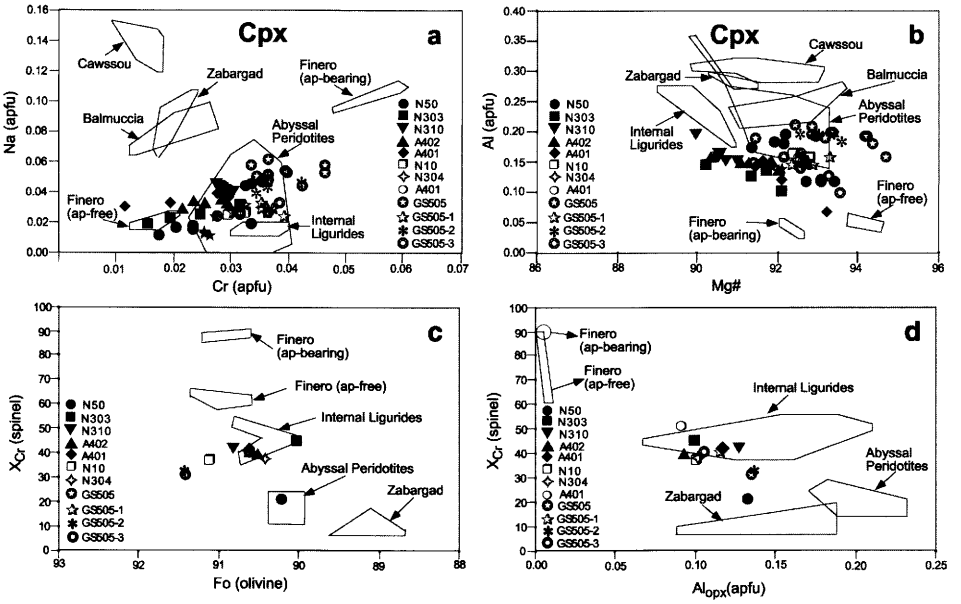

Fig. 8. Major element variability of minerals from Nurali and Mindyak peridotites (P. Spadea, unpublished data). (**a**) and (**b**) show the clinopyroxene composition, and the compositional fields of reference clinopyroxene from: (1) subcontinental, fertile, spinel lherzolites (Balmuccia massif, Western Alps, Italy, Rivalenti *et al.* 1995; Zabargad peridotite–pyroxenite association, Bonatti *et al.* 1986; Piccardo *et al.* 1988); (2) spinel peridotites recrystallized by impregnation of alkaline melts (Caussou massif; Eastern Pyrenees, France, Fabriès *et al.* 1989); (3) abyssal peridotites (Johnson *et al.* 1990); (4) ophiolites related to the Jurassic Ligurian–Piedmontese Ocean (Northern Apennines, Italy; Rampone *et al.* 1996); (5) orogenic massifs variably depleted by partial melting events, followed by metasomatic enrichments, in supra-subduction mantle-wedge environment (Finero massif, Western Alps, Zanetti *et al.* 1999). (**c**) and (**d**) document the relationships of spinel composition with Fo content of olivine and Al content of orthopyroxene. The plotted values of the Nurali and Mindyak minerals are the average composition of several spinel, olivine and orthopyroxene analyses for each sample. Only the composition of orthopyroxene with CaO <1 wt% has been used for (**d**).

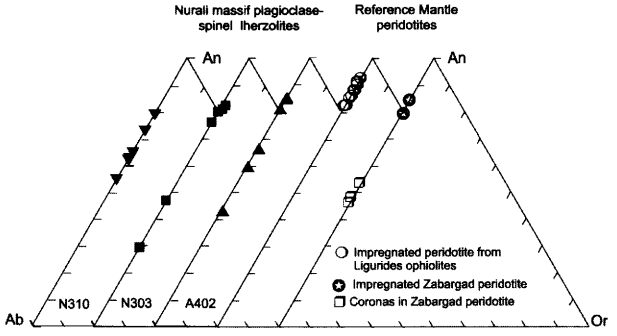

Fig. 9. Major element composition of plagioclase from Nurali lherzolites (P. Spadea, unpublished data). For comparison, we show the composition of plagioclase from: (1) melt-impregnated ophiolites related to the Jurassic Ligurian–Piedmontese Ocean (Italy and Corsica, Rampone *et al.* 1997); (2) melt-impregnated transitional peridotites from Zabargad Island (near the African margin of the Red Sea, Piccardo *et al.* 1988); (3) Zabargad spinel lherzolites with plagioclase coronas around spinel, as a result of incipient sub-solidus recrystallization at the spinel- to plagioclase-facies transition (Piccardo *et al.* 1988).

found in clinopyroxenes from residual oceanic peridotites (Johnson *et al.* 1990; Johnson & Dick 1992) and from peridotites belonging to ophiolitic sequences (e.g. Internal Ligurides, Northern Apennines, Italy, Rampone *et al.* 1996). On the other hand, similar features are also displayed by clinopyroxenes from orogenic peridotites commonly ascribed to the subcontinental realm (e.g. Baldis-

Table 3. *Trace element compositions (ppm element, except TiO_2 as wt%) of minerals from Nurali and Midyak mantle peridotites determined with laser-ablation microprobe ICP-MS*

	Nurali massif													
Sample:	N50 Plagioclase–spinel lherzolite				N303 Plagioclase–spinel lherzolite									
Mineral:	Cpx	Cpx	Cpx	Opx	Cpx	Cpx	Cpx	Cpx	Opx	Opx	Opx	Opx	Opx	Opx
Site:	D6	D2	D5	D9	2core1	2core2	1Brim	1Acore	A5A	A5B	B7A	B8	B9A	B9C
Sc	63	77	75	22	71	77	72	78	29	31	27	28	25	26
TiO_2	0.66	0.66	0.65	0.16	0.32	0.34	0.35	0.40	0.073	0.087	0.086	0.108	0.095	0.104
V	288	324	323	114	291	312	382	442	133	141	129	142	130	127
Cr	5118	5919	6107	2704	5149	5104	5825	7167	3958	3899	3564	4489	4139	4053
Rb	n.d.	n.d.	n.d.	n.d.	n.d.	n.d.	n.d.	n.d.	n.d.	n.d.	n.d.	n.d.	n.d.	n.d.
Sr	1.55	1.22	2.01	n.d.	0.40	0.46	0.31	0.52	n.d.	n.d.	n.d.	n.d.	n.d.	n.d.
Y	26.8	23.7	22.4	1.94	17.4	20.8	19.2	20.6	1.51	1.92	1.68	1.81	1.54	1.50
Zr	30	27	28	1.65	2.51	2.79	2.27	2.22	n.d.	0.18	0.19	0.27	0.23	0.26
Nb	n.d.	n.d.	n.d.	n.d.	0.04	0.05	0.06	0.08	n.d.	n.d.	n.d.	n.d.	n.d.	n.d.
Ba	n.d.	n.d.	n.d.	n.d.	0.07	0.05	<0.03	0.05	n.d.	n.d.	n.d.	n.d.	n.d.	n.d.
La	0.18	0.17	0.15	n.d.	0.011	0.016	0.031	0.020	n.d.	n.d.	n.d.	n.d.	n.d.	n.d.
Ce	1.60	1.43	1.38	n.d.	0.13	0.17	0.19	0.24	n.d.	n.d.	n.d.	n.d.	n.d.	n.d.
Pr	0.51	0.45	0.44	n.d.	0.079	0.073	0.086	0.066	n.d.	n.d.	n.d.	n.d.	n.d.	n.d.
Nd	3.9	3.7	3.0	0.002	0.76	0.97	0.89	1.10	n.d.	0.002	n.d.	n.d.	n.d.	0.003
Sm	2.16	2.05	1.88	n.d.	0.96	0.99	1.07	1.15	0.004	n.d.	0.005	n.d.	n.d.	n.d.
Eu	0.90	0.66	0.75	n.d.	0.37	0.39	0.43	0.44	n.d.	n.d.	n.d.	n.d.	n.d.	0.005
Gd	3.3	3.5	3.3	n.d.	1.72	2.00	1.81	1.99	n.d.	n.d.	n.d.	n.d.	n.d.	n.d.
Tb	0.62	0.62	0.57	0.033	0.38	0.43	0.44	0.48	n.d.	0.011	n.d.	0.015	0.011	0.014
Dy	4.4	4.1	4.3	0.21	3.0	3.1	3.6	3.7	0.17	0.19	0.20	0.20	0.15	0.15
Ho	0.90	0.85	0.87	0.060	0.70	0.73	0.76	0.79	0.054	0.062	0.054	0.075	0.050	0.070
Er	2.57	2.36	2.20	0.25	1.79	2.40	2.23	2.56	0.24	0.30	0.28	0.34	0.23	0.18
Tm	0.38	0.33	0.33	0.049	0.25	0.32	0.33	0.31	0.050	0.061	n.d.	0.056	n.d.	0.041
Yb	2.02	1.87	1.83	0.36	1.60	1.99	2.36	2.10	0.36	0.56	0.41	0.55	0.40	0.47
Lu	0.28	0.26	0.25	0.060	0.24	0.27	0.27	0.37	0.079	0.066	0.066	0.057	0.066	0.087
Hf	0.82	1.17	1.36	0.09	0.22	0.34	0.26	0.20	n.d.	n.d.	0.015	0.020	n.d.	n.d.
Ta	n.d.	n.d.	n.d.	n.d.	0.009	0.002	<0.002	0.009	n.d.	n.d.	n.d.	n.d.	n.d.	n.d.
Pb	n.d.	n.d.	n.d.	n.d.	<0.01	0.02	<0.02	<0.02	n.d.	n.d.	n.d.	n.d.	n.d.	n.d.
Th	n.d.	n.d.	n.d.	n.d.	0.001	0.001	0.004	0.002	n.d.	n.d.	n.d.	n.d.	n.d.	n.d.
U	n.d.	n.d.	n.d.	n.d.	0.001	0.0001	0.003	0.002	n.d.	n.d.	n.d.	n.d.	n.d.	n.d.

	Nurali massif													
Sample:	N310 Plagioclase–spinel lherzolite					A402 Plagioclase–spinel lherzolite					N304 Spinel lherzolite			
Mineral:	Cpx	Cpx	Cpx	Cpx	Opx	Cpx	Cpx	Cpx	Opx	Opx	Cpx	Cpx	Cpx	Cpx
Site	B15	B16	B13	B11	B14	B23	B18	B20	B17	B24	C3	C4A	C4B	C8
Sc	72	73	62	83	26	64	72	71	25	22	83	85	93	85
TiO_2	0.28	0.34	0.29	0.38	0.08	0.16	0.20	0.19	0.06	0.05	0.14	0.15	0.16	0.16
V	296	333	283	353	126	233	271	268	109	97	270	270	276	305

(*continued overleaf*)

Table 3. (*continued*)

	Nurali massif													
Sample:	N50 Plagioclase–spinel lherzolite				N303 Plagioclase–spinel lherzolite									
Mineral:	Cpx	Cpx	Cpx	Opx	Cpx	Cpx	Cpx	Cpx	Opx	Opx	Opx	Opx	Opx	Opx
Site:	D6	D2	D5	D9	2core1	2core2	1Brim	1Acore	A5A	A5B	B7A	B8	B9A	B9C
Cr	7701	6919	7276	7552	4721	7850	7974	8028	4102	3705	6514	6697	6261	7283
Rb	n.d.	n.d.	n.d.	n.d.	n.d.	n.d.	n.d.	n.d.	n.d.	n.d.	n.d.	n.d.	n.d.	n.d.
Sr	0.35	0.25	0.39	0.36	n.d.	0.09	0.10	0.09	n.d.	0.11	3.0	2.57	3.0	2.43
Y	17.4	19.8	17.3	25.5	1.91	13.86	16.89	16.49	1.36	1.13	7.4	6.8	7.0	7.1
Zr	1.82	2.48	1.85	3.00	0.23	0.42	0.57	0.56	n.d.	n.d.	1.25	1.12	1.31	1.10
Nb	n.d.	n.d.	n.d.	n.d.	n.d.	n.d.	n.d.	n.d.	n.d.	n.d.	n.d.	n.d.	n.d.	n.d.
Ba	n.d.	n.d.	n.d.	n.d.	n.d.	n.d.	n.d.	n.d.	n.d.	n.d.	n.d.	n.d.	n.d.	n.d.
La	n.d.	n.d.	n.d.	0.012	n.d.	n.d.	n.d.	n.d.	n.d.	n.d.	0.030	0.023	0.051	0.020
Ce	0.060	0.062	0.067	0.070	n.d.	0.010	0.010	0.010	n.d.	n.d.	0.16	0.12	0.18	0.13
Pr	0.046	n.d.	0.050	0.062	n.d.	0.011	0.015	0.013	n.d.	n.d.	0.045	0.044	0.039	0.041
Nd	0.73	0.71	0.71	0.93	n.d.	0.24	0.24	0.25	0.003	n.d.	0.42	0.35	0.41	0.38
Sm	0.95	0.89	0.97	1.04	n.d.	0.49	0.56	0.54	n.d.	0.006	0.33	0.26	0.30	0.31
Eu	0.37	0.44	0.36	0.43	n.d.	0.26	0.24	0.28	n.d.	n.d.	0.12	0.14	0.16	0.13
Gd	1.94	2.02	1.67	2.29	n.d.	1.36	1.61	1.62	n.d.	n.d.	0.71	0.68	0.76	0.73
Tb	0.41	0.43	0.37	0.51	0.020	0.28	0.35	0.35	n.d.	0.009	0.16	0.18	0.17	0.18
Dy	2.7	3.1	2.84	4.0	0.18	2.22	2.75	2.40	0.12	0.11	1.14	1.15	1.11	1.09
Ho	0.67	0.77	0.63	0.94	0.065	0.55	0.60	0.55	0.045	0.033	0.27	0.26	0.26	0.25
Er	1.80	2.14	1.92	2.59	0.30	1.51	1.85	1.65	0.20	0.14	0.82	0.75	0.78	0.76
Tm	0.28	0.30	0.27	0.41	0.046	0.21	0.26	0.21	0.052	0.040	0.13	0.13	0.13	0.13
Yb	1.79	2.05	1.79	2.44	0.45	1.45	1.60	1.45	0.35	0.29	0.68	0.74	0.71	0.74
Lu	0.26	0.30	0.25	0.31	0.10	0.19	0.22	0.23	0.059	0.059	0.11	0.11	0.085	0.10
Hf	0.28	0.32	0.26	0.34	0.045	0.09	0.11	0.09	0.012	0.023	0.040	0.10	0.076	0.076
Ta	n.d.	n.d.	n.d.	n.d.	n.d.	n.d.	n.d.	n.d.	n.d.	n.d.	n.d.	n.d.	n.d.	n.d.
Pb	n.d.	n.d.	n.d.	n.d.	n.d.	n.d.	n.d.	n.d.	n.d.	n.d.	n.d.	n.d.	n.d.	n.d.
Th	n.d.	n.d.	n.d.	n.d.	n.d.	n.d.	n.d.	n.d.	n.d.	n.d.	0.001	0.004	0.001	0.0003
U	n.d.	n.d.	n.d.	n.d.	n.d.	n.d.	n.d.	n.d.	n.d.	n.d.	0.001	0.001	0.001	<0.001

	Nurali massif									Mindyak massif					
Sample:	A403 Spinel harzburgite				A404 Spinel harzburgite					GS505 Spinel lherzolite					
Mineral:	Cpx	Cpx	Opx	Opx	Cpx	Cpx	Cpx	Opx	Amph	Cpx	Cpx	Cpx	CpxB	CpxB	Opx
Site:	B25A	B25B	B26A	B26B	B36	B34A	B34B	B30	B33	D15	D11A	D10A	D10	D11	D12
Sc	60	62	20	20	73	85	94	19	64	51	55	54	53	57	18
TiO_2	0.26	0.24	0.08	0.08	0.06	0.07	0.07	0.02	0.11	0.21	0.22	0.22	0.21	0.22	0.07
V	225	226	85	88	193	221	227	67	203	223	226	214	210	221	88
Cr	12322	11415	3941	4167	9926	9542	9240	4249	8051	10455	10911	9551	9960	10033	5050
Rb	n.d.	n.d.	n.d.	n.d.	n.d.	n.d.	n.d.	n.d.	0.37	n.d.	n.d.	n.d.	n.d.	n.d.	n.d.
Sr	10.9	10.9	n.d.	0.12	22	23	26	0.19	18	29	28	28	27	30	0.16
Y	9.9	10.1	0.82	0.70	3.0	2.98	3.4	0.21	2.45	10.1	9.7	10.2	10.3	10.2	0.79
Zr	7.1	7.3	0.45	0.46	28	29	30	1.26	24	13	15	15	15	16	1.14
Nb	n.d.	n.d.	n.d.	n.d.	0.11	0.42	0.28	n.d.	15	<0.03	<0.05	<0.03	<0.03	<0.04	n.d.
Ba	n.d.	n.d.	n.d.	n.d.	n.d.	n.d.	n.d.	n.d.	13	<0.26	<0.25	<0.15	0.12	0.24	n.d.
La	0.11	0.12	n.d.	n.d.	0.70	0.82	0.79	n.d.	0.59	0.76	0.73	0.67	0.70	0.81	n.d.
Ce	0.75	0.72	0.006	0.003	2.72	2.71	3.07	n.d.	2.14	2.65	2.30	2.46	2.49	2.58	0.023

Pr	0.30	0.28	n.d.	n.d.	0.57	0.59	0.55	n.d.	0.40	0.49	0.43	0.44	0.44	0.50	0.007
Nd	2.58	2.39	0.002	0.005	3.1	3.1	3.7	0.004	2.40	2.91	2.48	2.68	2.57	2.83	0.046
Sm	1.49	1.36	0.018	n.d.	0.93	0.88	1.06	n.d.	0.68	1.12	1.08	1.04	1.08	1.14	n.d.
Eu	0.55	0.60	n.d.	n.d.	0.33	0.36	0.35	n.d.	0.21	0.49	0.41	0.47	0.49	0.48	n.d.
Gd	2.16	2.25	n.d.	n.d.	0.76	0.85	0.88	n.d.	0.64	1.55	1.56	1.60	1.56	1.46	n.d.
Tb	0.35	0.33	0.018	n.d.	0.10	0.12	0.13	n.d.	0.094	0.26	0.26	0.27	0.29	0.27	n.d.
Dy	2.15	1.98	0.14	0.127	0.70	0.67	0.72	0.018	0.48	1.76	1.44	1.60	1.76	1.69	0.041
Ho	0.38	0.36	0.031	0.039	0.13	0.13	0.14	n.d.	0.082	0.39	0.34	0.35	0.38	0.38	0.032
Er	1.04	0.90	0.08	0.080	0.29	0.32	0.31	0.025	0.30	1.01	0.89	1.05	1.02	1.02	0.10
Tm	0.13	0.12	0.017	0.016	0.05	0.04	0.04	n.d.	n.d.	n.d.	n.d.	0.16	0.14	0.14	0.02
Yb	0.74	0.66	0.16	0.121	0.38	0.34	0.20	n.d.	0.29	0.91	0.95	0.95	1.00	0.92	0.15
Lu	0.10	0.09	0.029	0.038	0.05	0.05	0.06	0.016	0.045	0.14	0.11	0.13	0.12	0.12	0.03
Hf	0.57	0.43	0.012	n.d.	0.88	0.92	0.87	0.06	0.62	0.47	0.50	0.73	0.59	0.61	0.06
Ta	n.d.	n.d.	n.d.	n.d.	0.043	0.085	n.d.	n.d.	0.73	0.02	<0.03	<0.02	<0.03	<0.03	n.d.
Pb	n.d.	n.d.	n.d.	n.d.	n.d.	n.d.	n.d.	n.d.	n.d.	n.d.	n.d.	n.d.	n.d.	n.d.	n.d.
Th	0.006	0.006	n.d.	n.d.	0.030	0.038	0.035	n.d.	0.018	0.017	0.016	0.013	0.011	0.006	0.003
U	0.003	<0.004	n.d.	n.d.	0.013	0.008	0.011	n.d.	<0.015	0.003	0.015	0.004	0.002	0.010	0.0004

	Mindyak massif								
Sample:	GS505-1 Spinel harzburgite					GS505-3 Spinel harzburgite			
Mineral:	Cpx	Cpx	Cpx	Opx	Opx	Cpx	Opx	Opx	Opx
Site:	D26B	D27	D22	D24	D25B	D16	D17	D19	D20
Sc	50	54	50	19	18	49	21	20	18
TiO_2	0.07	0.07	0.07	0.03	0.03	0.19	0.07	0.08	0.08
V	165	158	162	74	68	187	78	79	77
Cr	9194	7785	8910	5467	5306	8716	4027	4638	4559
Rb	n.d.	n.d.	n.d.	n.d.	n.d.	n.d.	n.d.	n.d.	n.d.
Sr	27	24	23	0.23	0.30	16	<0.14	<0.09	<0.09
Y	2.64	3.1	3.0	0.32	0.29	6.5	0.53	0.61	0.55
Zr	1.80	1.65	1.82	0.24	0.15	7.1	0.57	0.54	0.52
Nb	n.d.	n.d.	n.d.	n.d.	n.d.	<0.05	<0.06	<0.04	<0.03
Ba	n.d.	n.d.	n.d.	n.d.	n.d.	<0.25	n.d.	n.d.	n.d.
La	0.35	0.31	0.23	n.d.	n.d.	0.25	n.d.	n.d.	n.d.
Ce	1.23	1.18	1.06	0.011	0.011	1.03	n.d.	n.d.	n.d.
Pr	0.22	0.21	0.20	n.d.	n.d.	0.23	n.d.	n.d.	n.d.
Nd	1.14	1.03	1.06	n.d.	n.d.	1.55	n.d.	n.d.	n.d.
Sm	0.34	0.30	0.36	n.d.	n.d.	0.74	n.d.	n.d.	n.d.
Eu	0.13	0.12	0.10	n.d.	n.d.	0.27	n.d.	n.d.	n.d.
Gd	0.46	n.d.	0.42	n.d.	n.d.	0.86	n.d.	n.d.	n.d.
Tb	0.08	0.06	0.08	n.d.	n.d.	0.17	n.d.	n.d.	0.009
Dy	0.51	0.42	0.54	n.d.	0.038	1.07	n.d.	n.d.	n.d.
Ho	0.11	0.10	0.12	n.d.	0.010	0.24	0.029	0.027	0.021
Er	0.33	0.29	0.38	0.082	0.076	0.59	0.100	0.098	0.099
Tm	0.05	n.d.	n.d.	0.018	n.d.	0.08	n.d.	n.d.	n.d.
Yb	0.34	0.26	0.46	0.13	0.11	0.59	0.179	0.188	0.171
Lu	0.05	n.d.	0.07	0.027	0.019	0.08	0.026	0.029	0.020
Hf	0.07	0.05	<0.10	0.01	n.d.	0.36	<0.07	0.04	0.01
Ta	n.d.	n.d.	n.d.	n.d.	n.d.	<0.04	n.d.	n.d.	n.d.
Pb	n.d.	n.d.	n.d.	n.d.	n.d.	<0.3	n.d.	n.d.	n.d.
Th	<0.003	<0.008	<0.004	n.d.	n.d.	0.004	n.d.	n.d.	n.d.
U	0.003	0.002	0.001	n.d.	n.d.	n.d.	n.d.	n.d.	n.d.

n.d., below detection limit.

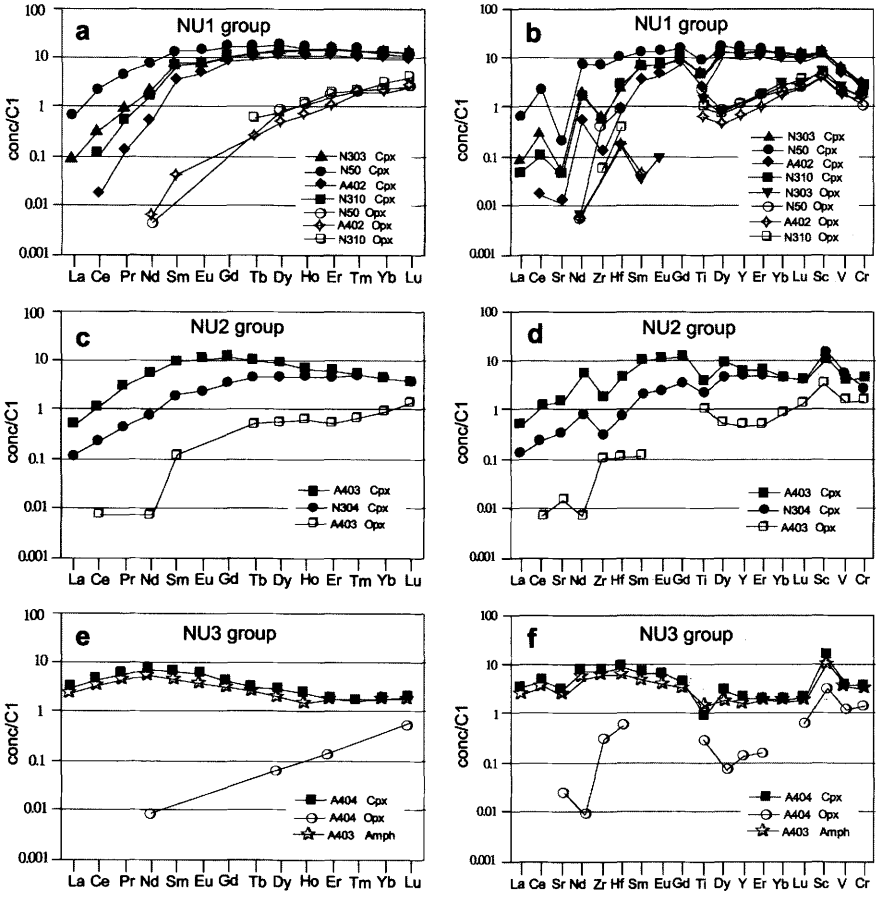

Fig. 10. C1-normalized (Anders & Grevesse 1989) REE patterns (**a**, **c**, **e**) and extended spider diagrams (**b**, **d**, **f**) for pyroxene and amphibole of Nurali peridotites.

sero massif and Balmuccia massif; Rivalenti *et al.* 1995; Mazzucchelli *et al.* 1999).

Nurali Group 2 consists of the clinopyroxenes from the N304 spinel lherzolite and the A403 spinel harzburgite. The REE patterns of the clinopyroxenes from these two samples (Fig. 10c) are significantly different in terms of LREE–MREE abundance and fractionation (Ce_N/Yb_N 0.06–0.28 Sm_N/Yb_N 0.46–2.27; Sm 0.3–1.43 ppm), but they are both characterized by similar low HREE content (*c.* 4–7 times C1), the absence of significant Sr anomaly, moderately negative Ti and Zr(Hf) anomaly, and similar Th(U)/La ratios (Fig. 10d). Johnson *et al.* (1990) reported trace element fractionation similar to that shown by the clinopyroxenes from spinel lherzolite N30 for clinopyroxenes from hotspot-proximal oceanic peridotites.

Nurali group 3 is represented by the clinopyroxenes from the A404 spinel harzburgite. They show LREE–MREE-enriched convex-upward patterns (Ce_N/Yb_N 2–4; Sm_N/Yb_N 2.7–5.7; Yb_N 1–2) (Fig. 10e), with no significant Zr and Hf anomaly, slightly negative Sr anomaly and negative Ti anomaly (Fig. 10f). The relative enrichment in LREE–MREE is accompanied by significant contents of even the most incompatible elements (Nb, Ta, Th and U). Consistent characteristics are shown by the associated amphibole, which is particularly enriched in Nb (15 ppm) and Ta (0.7 ppm) with respect to the clinopyroxenes. However, the amphibole/clinopyroxene compositional ratios for Sr (0.8), Ti (1.8), Y (0.8) and REE (minimum value 0.6 for Eu) are low for pairs from mantle ultramafic rocks (see, e.g. the compilation reported by Vannucci *et al.* 1995). This suggests that chemical equilibrium was not attained between the two minerals and/or their crystallization occurred under particular thermochemical conditions. The LREE/HREE, Nb(Ta)/LREE and Ba/LREE ratios of the clinopyroxene and amphibole from the spinel harzburgite A404

(Fig. 10e and f) are strictly similar to their magmatic analogues in equilibrium with alkaline melts (Irving & Frey 1984; Zanetti *et al.* 1995, 1996) and have been also documented in clinopyroxenes belonging to spinel harzburgite xenoliths from the Massif Central, France (Xu *et al.* 1998) and Pali Aike Volcanic Field, South Patagonia, Argentina (Vannucci *et al.* 2002).

Mindyak peridotite. The trace element content of the clinopyroxenes from the Mindyak peridotites is broadly correlated with their fertility, being higher in the spinel lherzolite GS505 than in the spinel harzburgites (GS505-1 and GS505-3). On the other hand, the Mindyak clinopyroxenes analysed in this study are homogeneously characterized by slightly to moderately LREE-depleted patterns (Ce_N/Yb_N 0.47–0.89), which are nearly flat to slightly convex-upward in the MREE–HREE region (Sm_N/Yb_N 0.58–1.4; Yb_N 2.2–5.8) (Fig. 11a). The Sr content is in the range of 16–30 ppm, and results in slightly negative to positive anomalies with respect to the adjacent REE (Fig. 11b). Zr and Hf contents are low in the GS505 spinel lherzolite (average 15 and 0.6 ppm, respectively), to very low in the GS505-1 harzburgite (average 1.8 and 0.06 ppm, respectively); as a result, they display negative anomalies, which deepen with a decrease in REE content. It is noteworthy that also the content of incompatible to compatible elements, such as Ti, V and Cr, is positively correlated with the REE variation.

The clinopyroxenes from the Mindyak lherzolites show some geochemical affinity in trace element composition to Nurali Group 2, namely low Ti, Y and HREE content and Zr(Hf)/LREE ratio, along with Sr/LREE close to one. On the other hand, the clinopyroxenes from the GS505-1 harzburgite have Ti, Y and HREE contents very similar to those of Nurali Group 3.

Orthopyroxene

Orthopyroxene shows the typical linearly fractionated LREE–MREE-depleted patterns (Figs 10 and 11). Consistent with the associated clinopyroxene, it has very low concentrations of the highly incompatible trace elements (e.g. Th, Nb and LREE), frequently close to or below the detection limits. Therefore, variations of these elements cannot be monitored adequately. On the contrary, the content of moderately incompatible to compatible elements (such as HREE, Y, V, Sc and Cr) is appreciable and can be compared with that of the associated clinopyroxenes. As a whole, all these elements are positively correlated for the two

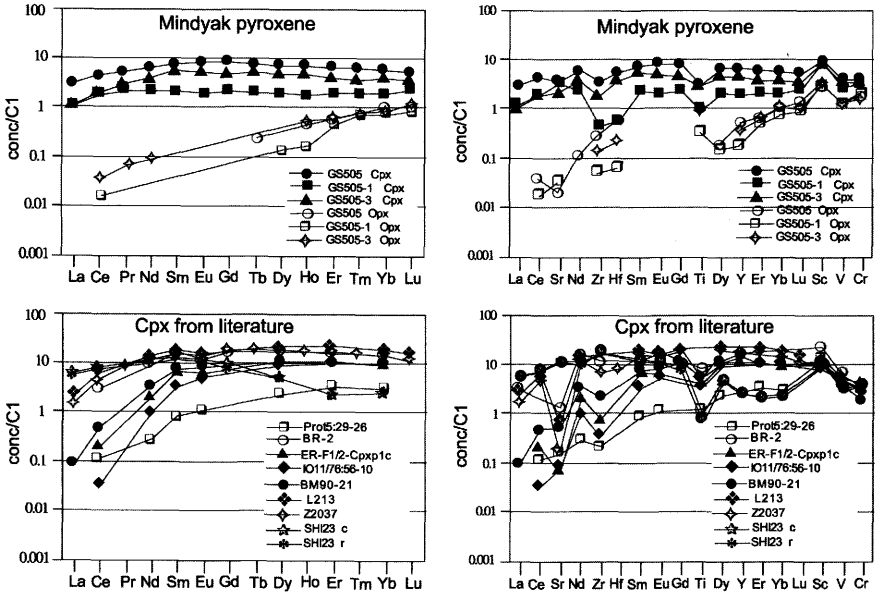

Fig. 11. C1-normalized (Anders & Grevesse 1989) REE patterns (**a**) and extended spider diagrams (**b**) for pyroxene of Mindyak peridotites. Literature data are plotted in (**c**) and (**d**) for clinopyroxene from: (1) abyssal peridotites (Prot5:29-26 and IO11/76:56-10; Johnson *et al.* 1990); (2) ophiolitic peridotites (cpx ER-F1/2-Cpxp1c is from Internal Ligurides, Northern Apennines, Rampone *et al.* 1996); (3) transitional realm (cpx BR-2; Bracco unit, Liguride Alps; Rampone *et al.* 1997; cpx L213, Lanzo massif, Western Alps, Bodinier *et al.* 1991; cpx Z2037; plagioclase Zabargad peridotite, Red Sea, A. Zanetti, unpublished data).

pyroxenes. V, Y and Ti show the strongest correlation, but HREE and Zr are also well correlated. A slight spread in correlation is displayed by Cr, Sc and Hf (with the last strongly biased by its low concentration in the orthopyroxene).

Petrogenesis of the Nurali and Mindyak peridotites

T and P estimates

The significant variability of texture, mineral assemblage and mineral composition reveals that the Nurali and Mindyak peridotites experienced a multistage evolution under largely different T and P conditions. According to Gasparik (1984) and Brey & Kohler (1990), if the Ca-richest compositions found in the orthopyroxene of the Mindyak peridotites actually document early stages of the thermal evolution of the massif, this latter would have experienced equilibrium T close to 1350 °C. This corresponds to the anhydrous spinel-facies peridotite solidus at P *c.* 1.5 GPa (Kinzler 1997). Similar T can be estimated on the basis of the Ca-richest orthopyroxene compositions found in the N310 plagioclase ± spinel lherzolite of the Nurali massif. On the other hand, the most abundant population of pyroxene by far consists of Ca-poor orthopyroxene (CaO <1 wt%) and Ca-rich clinopyroxene (CaO >23 wt%). The equilibrium T estimated for these pyroxenes is in the range 830–950 °C using the geothermometers based on the enstatite–diopside solvus (Wells 1977; T_{BKN}, Brey & Kohler 1990), whereas a higher T range, 960–1070 °C, can be estimated on the basis of Ca partitioning (T_{Ca}, Brey & Kohler 1990). Consistent T (850–1000 °C) is also found for the spinel-facies peridotites using the geothermometer of Witt-Eickschen & Seck (1991), thus suggesting the presence of chemical equilibrium between spinel and low-T pyroxene. These temperatures are probably related to the steady-state equilibrium under mantle (both spinel- and plagioclase-facies) conditions.

The textural features of the plagioclase in the Nurali lherzolites (N50, N303, N310, A402 and A401) indicate that they suffered an extensive recrystallization at low P (<0.8 GPa). The maximum P of the spinel-facies peridotites from Mindyak, estimated on the basis of the spinel composition (Webb & Wood 1986), is in the range of 2.2–2.3 GPa. These values are very similar to those estimated for spinel-facies peridotites from Nurali (2.3–2.5 GPa), but are not consistent with the low Ca contents of the associated olivine, which suggest low equilibrium P (≤1.0 GPa; geobarometer by Brey & Kohler 1990).

Information on the equilibrium T can be also obtained by the application of the empirical equations of Seitz *et al.* (1999), which are based on the orthopyroxene–clinopyroxene partitioning for V, Sc and Cr. The T range estimated on the basis of V partitioning (T_V) is by far the smallest (assuming P is 0.8 GPa, T_V is 1120–1150°C for the Mindyak pairs, 1090–1120°C for the Nurali Group 1–Group 2 pairs, and 1040°C for Nurali Group 3 pairs). The T_{Sc} values correlate significantly with the corresponding T_V (assuming P is 0.8 GPa, T_{Sc} is 1060–1120 °C for the Mindyak pairs, 1030–1090 °C for the Nurali Group 1–Group 2 group pairs and 950 °C for A404 pairs), but they are generally *c.* 45 °C higher than T_V. The T values calculated on the basis of Cr partitioning (T_{Cr}) are much more variable, encompassing the ranges of both T_V and T_{Sc} The large T_{Cr} variability is associated with a significant variation of the Cr content in the pyroxene, which probably reflects local incomplete sub-solidus equilibrium. As a whole, the T values obtained on the basis of V and Sc partitioning among pyroxenes are significantly higher than those calculated on the basis of major elements, thus suggesting different closure T for the relative exchange reactions.

The origin of plagioclase

The presence of plagioclase in mantle peridotites has been attributed to sub-solidus recrystallization of spinel-facies assemblages at P lower than 0.8 GPa and to the crystallization of interstitial melts, either of exotic origin or entrapped after partial melting of the host peridotite. The variable textural features and major element mineral chemistry of the plagioclase from the Nurali peridotites reveal that both of these plagioclase-forming processes probably occurred. In particular, the high-An (80–85) interstitial plagioclase randomly distributed or aligned in pseudo-veins is typical of peridotites impregnated by strongly LREE-depleted melts (Rampone *et al.* 1997), and can be therefore related to such a process. Conversely, some large low-An (<50) plagioclases overgrowing the spinel relics are probably derived by spinel breakdown at low P, possibly in the presence of a Na-rich (late?) metasomatic agent. Further petrographical and chemical investigations are needed to understand whether or not the two processes were genetically related (e.g. the sub-solidus recrystallization of spinel could have been triggered by the presence of interstitial melts).

Noticeably, the extensive recrystallization that the spinel underwent and the evolved nature of the plagioclase-bearing aggregates after spinel are consistent with advanced re-equilibration of these peridotites under plagioclase-facies conditions.

This represents a distinctive feature with respect to subcontinental peridotites involved in oceanization processes that contain plagioclase forming fine-grained, narrow coronas around spinel (e.g. fertile lherzolites from Zabargad peridotites, External Ligurides Units; Rampone *et al.* 1993). In contrast, the spinel–plagioclase relations of the plagioclase-bearing Nurali peridotites provide evidence for a long-term residence under low-*P* mantle conditions, before their emplacement at the surface.

Whole-rock vs. pyroxene chemistry

It has been well documented and deeply debated in previous papers (Salters & Shimizu 1988; Rampone *et al.* 1991, 1996; McDonough *et al.* 1992) that the content and the fractionation of LREE–REE and Sr of bulk-rock composition of spinel-facies mantle peridotites can be confidently estimated on the basis of clinopyroxene composition. In contrast, the HREE, Zr, Ti, Sc and V budget is significantly influenced by the orthopyroxene contribution, and Cr mass-balance calculation requires the involvement of spinel. The comparison between the trace element composition of the pyroxenes from the Nurali and Mindyak peridotites and the respective bulk-rock composition show significant positive correlation for MREE–HREE, Y, Ti, Sc and V. The correlation for Cr is positive but somewhat spread, confirming the important role played by spinel in its budget. It is noteworthy that clinopyroxenes and bulk rock show very poor to no correlation for LREE and Sr content. This mismatch can be of various origins. In particular, the higher LREE and Sr content, and the larger LREE–HREE value shown by the bulk rock with respect to the clinopyroxenes could be explained by the presence of interstitial plagioclase (given that this mineral shows a typical LREE-enriched pattern, e.g. Cortesogno *et al.* 2000) and later interstitial components. Some plagioclase-free, spinel lherzolites and spinel harzburgites from both Mindyak and Nurali massif (e.g. samples GS505-1, GS505-3, N304) also display a higher LREE–HREE value with respect to the clinopyroxenes. Conversely, their LREE and Sr content is always markedly lower than that of clinopyroxenes. The lack of petrographical evidence of the presence of minerals stable in the spinel-facies assemblage and able to host significant amount of LREE (e.g. apatite) could relate these LREE enrichments to late, low-*T*, alteration processes. In particular, the role of secondary alteration in determining U-shaped REE patterns in the bulk rock has been previously assessed for peridotites from the Trinity ophiolite complex (Gruau *et al.* 1998).

Evidence for partial melting and melt flow processes

Mindyak peridotites. The low bulk-rock contents of moderately incompatible elements such as Al, Ca, Na, HREE, Y and Ti, together with high Mg contents, suggest that all the Mindyak peridotites analysed in this study underwent large degrees of partial melting. This is confirmed by the pyroxene composition, which displays the same characteristics as the bulk rock, particularly a high Cr content. The bulk-rock HREE contents of the Mindyak lherzolites and harzburgites are consistent with 11% and 14–15% of fractional melting, respectively. Similarly, the HREE content of clinopyroxene indicates 9–12% of partial (fractional) melting for the lherzolites and 15% for the GS505-1 harzburgite.

Conversely, the slightly LREE-depleted to nearly flat REE patterns shown by the clinopyroxenes and the overall Fe-enriched composition of the spinel harzburgite minerals cannot be explained by simple partial melting processes, but require the addition of LREE–MREE-enriched component during or after the melting events. An alternative working hypothesis is that both mineralogical and chemical differences between harzburgites and lherzolites could be a direct result of reactive porous flow percolation of melts in different sectors of the mantle column.

Consistent with the LREE–HREE fractionation, the Ti/Zr ratios of the Mindyak clinopyroxenes are too low to be explained by partial melting (see, e.g. the modelling of the variation of Ti/Zr ratio during different regimes of partial melting reported by Johnson *et al.* 1990). This indicates that percolating melts reset also the Zr (Hf) composition (Kelemen *et al.* 1992, 1995).

The trace element composition of the hypothetical melts percolating the Mindyak peridotites can be estimated on the basis of the clinopyroxene composition and appropriate clinopyroxene–liquid partition coefficients for basaltic systems ($D^{cpx/L}$). The melts calculated in equilibrium with the spinel lherzolites clinopyroxenes exhibit LREE-enriched patterns (La_N/Sm_N 1.2–3; La_N/Yb_N 2–4.7), slightly negative to slightly positive Sr anomaly, zero to positive Zr anomaly ($D^{cpx/Basalt}$ from Hart & Dunn 1993; Skulski *et al.* 1994) and low Th_N/La_N ratios (*c.* 0.4, with a $D_{Th}^{cpx/Basalt}$ of 0.02 calculated on the basis of Al^{IV} content of the Mindyak clinopyroxenes using the empirical equations proposed by Lundstrom *et al.* (1994)). In particular, the low $Th_N/LREE_N$ can be diagnostic for constraining the geochemical nature of the percolating melts. In fact, Th_N/La_N is typically 0.4 in normal mid-ocean ridge basalt (N-MORB; Hofmann 1988), with most alkaline magmas hav-

ing $Th_N(U_N)/La_N$ *c.* 1 (e.g. Halliday *et al.* 1995) and calc-alkaline magmas having values from slightly less than one to significantly greater than one (e.g. Conrey *et al.* 1997; Smith *et al.* 1997). This ratio should increase during the melt–peridotite interaction, owing to the larger La compatibility with respect to Th in the mantle peridotites. Consistently, Th_N/La_N values from slightly less than one to significantly greater than one, as recognized in most clinopyroxenes from metasomatized peridotites related to the Patagonian mantle wedge that interacted with slab-derived components (Ciuffi *et al.* 2001; Laurora *et al.* 2001) and to the lithospheric mantle beneath the Morocco continental rifting that interacted with alkaline, highly evolved melts (Raffone *et al.* 2001). As a consequence, the low Th_N/La_N must be an inherited character of the percolating melt and cannot be acquired by reactive porous flow. In particular, lavas of tholeiitic to transitional geochemical affinity show low Th_N/La_N along with $LREE_N/HREE_N > 1$ (e.g. Iceland plume, Hemond *et al.* 1993). In general, the low abundance of Nb and Ta (below the detection limits), along with the low Ba content, may provide further evidence in favour of a tholeiitic nature of the infiltrating melts.

Nurali Group 1 peridotites. The extreme REE fractionation shown by the clinopyroxenes of the Nurali N303, N310 and A402 lherzolites has been documented for clinopyroxenes of lherzolites from the oceanic realm (e.g. Johnson *et al.* 1990), ophiolitic sequences (Rampone *et al.* 1996; Rampone *et al.* 1997) and subcontinental mantle sectors (Rivalenti *et al.* 1995; Mazzucchelli *et al.* 1999). Clinopyroxenes with such geochemical signatures have been interpreted as a refractory phase after fractional or incremental melting processes (Johnson *et al.* 1990), or as a newly formed phase, crystallized in equilibrium with migrating (Rampone *et al.* 1997) or trapped (Seyler *et al.* 2001) melts, either single-step or incremental. On the other hand, the coarse, interstitial and/or symplectitic plagioclase of the Nurali lherzolites is typical of peridotites involved in oceanization processes *sensu lato*, namely, abyssal peridotites, ophiolitic sequences and thinned subcontinental lithosphere from transitional settings (e.g. the peridotite–pyroxenite association of Zabargad Island, Red Sea, Piccardo *et al.* 1988; Galicia margin, Cornen *et al.* 1996; Seifert & Brunotte 1996; Charpentier 2000). In contrast, to our knowledge, such plagioclase has never been observed in truly subcontinental peridotites.

In addition, the Nurali lherzolites share the following specific features with the abyssal and ophiolitic peridotites having clinopyroxenes with large LREE–HREE fractionation: (1) a relatively high modal clinopyroxene content (5–10 vol.%), in spite of their residual character; (2) a low to very low amount of highly incompatible to moderately incompatible elements, such as Sr, Zr, Ti and Na; (3) a lower depletion of moderately incompatible elements, such as Ca, Al and V.

Therefore, it can be concluded that all the mineralogical, petrographic and geochemical features suggest that the LREE-depleted, plagioclase-bearing Nurali lherzolites were involved in petrogenetic processes related to the formation of oceanic lithosphere.

In this frame, the microtextural features of Cpx1 and Cpx2 are regarded as critical points to constrain the specific petrological processes affecting the evolution of these peridotites. In particular, the Cpx1-bearing mineral assemblages can be regarded as residual after partial melting events. In contrast, the Cpx2-bearing mineral assemblage characterized by symplectitic textures and the presence of pseudo-veins of plagioclase can be interpreted as the reaction product between peridotite and impregnating melt (Rampone *et al.* 1997). Petrographic evidence indicates that the effects of impregnation are subordinate in the N401 and N402 lherzolites (where Cpx1 is abundant), intermediate in the N310 lherzolite, and dominant in the N303 lherzolite.

Theoretical modelling of the fractional melting process (Johnson *et al.* 1990) of a fertile spinel lherzolite indicates that the bulk-rock HREE content and fractionation of the N401 and N402 lherzolites are consistent with 6–8% melting of a fertile source under spinel-facies conditions. Instead, lower degrees of partial melting (3–5%) can be estimated for the N303 and N310 lherzolites. The bulk-rock LREE/HREE value is too large to be related to melting processes, and probably indicates the addition of relatively LREE-enriched melts or late fluids to the system. Interestingly, the HREE composition and fractionation of the clinopyroxenes are not strictly consistent with the degree of partial melting as deduced by the bulk rock. In particular, the LREE–HREE fractionation of the clinopyroxenes is indicative of relatively large melting degrees, whereas the HREE content argues in favour of limited melt extraction. Moreover, the LREE content of the clinopyroxenes provides melting estimates similar to those obtained on the basis of bulk-rock composition. This apparent inconsistency can be explained by sub-solidus redistribution of REE between plagioclase and clinopyroxene, mainly resulting in the increase of HREE content in clinopyroxene. Further support to this interpretation is provided by the large negative Sr anomaly of the clinopyroxenes, which

is not shown by the bulk-rock composition. The petrographic and geochemical considerations reported above permit us to assume as realistic the degrees of partial melting estimated for the N401 and N402 lherzolites, before the later impregnation event. However, the lower degrees of partial melting estimated for the N303 and 310 lherzolites are probably an artefact and reflect the chemical signatures of the impregnating melts. These latter are possibly regarded as incremental melts rather than MORB in the light of the extreme LREE–HREE fractionation shown by the clinopyroxenes from the N303 and N310 lherzolites.

Bulk-rock and mineral major element chemistry suggest that the N50 lherzolite experienced depletion to a limited extent (*c.* 3%). Similarly to the N303 lherzolite, this sample shows diffuse Cpx2-bearing symplectite and interstitial plagioclase. These features, along with the fertile REE composition of the clinopyroxenes and their strong negative Sr anomaly, suggest reaction with large volumes of impregnating melt and sub-solidus re-equilibration in the plagioclase stability field.

The overall trace element signatures of the clinopyroxenes indicate that the refertilization processes were operated by melts of MORB-like composition, as is the case for other occurrences elsewhere. Examples include: (1) the plagioclase-rich subcontinental peridotites of Zabargad Island (Piccardo *et al.* 2002), which experienced fracturing, melt impregnation and uplift, as a consequence of the oceanization process of the Red Sea area; (2) the plagioclase-bearing peridotites of the southern body of the Lanzo Massif (Western Alps), which also represents a section of the subcontinental lithosphere that underwent a polyphase history of partial melting and melt impregnation during continental rifting related to the opening of the Jurassic–early Cretaceous Piedmont–Ligurian ocean (Bodinier *et al.* 1991; Piccardo *et al.* 2002); (3) the Internal Ligurides peridotites from the Bracco Unit (Rampone *et al.* 1997).

Nurali Group 2 peridotites. The overall bulk-rock geochemical features of Group 2 peridotites, namely low HREE, Y, Ti and V, in association with LREE/HREE value significantly higher than in Group 1 peridotites, are uncommon for abyssal peridotites and ophiolitic sequences.

Trace element compositions of peridotite clinopyroxene from hotspot zones similar to those of the N304 spinel lherzolite clinopyroxenes have been interpreted by Johnson *et al.* (1990) as the result of a complex multistage evolution, involving: (1) relatively high degrees of fractional melting in the garnet stability field leaving residual garnet; (2) decompression reaction of garnet to form two-pyroxenes + spinel; (3) additional melting in the spinel stability field and exsolution of clinopyroxene from orthopyroxene.

If the partial melting of the A403 spinel harzburgite started under garnet-facies conditions, then the REE distribution of its clinopyroxene is consistent with low degrees of fractional melting (<5%). However, to avoid the redistribution of HREE to clinopyroxene during garnet breakdown and to preserve the convex-upward pattern of clinopyroxene, garnet is required to be completely exhausted during melting. Although possible, particularly at low pressure, this scenario is regarded as unlikely.

On the other hand, several mineralogical and geochemical features suggest that Group 2 peridotites underwent large melt percolation after or during a depletion processes. For example, the large modal clinopyroxene content of the N304 spinel lherzolite (15% by volume) cannot be reconciled with simple clinopyroxene formation via orthopyroxene exsolution. As for the A403 spinel harzburgite, the highly residual character of its bulk-rock major and trace element composition (e.g. the large Mg and the low Al, Ca and HREE concentrations) is not consistent with the relatively large MREE content of the clinopyroxenes.

A working alternative explanation is that the present mineralogical and geochemical features of Group 2 peridotites are inherited by pervasive melt percolation under spinel-facies conditions. The relationship between melt migration and partial melting processes is difficult to constrain because of the limited number of samples and their significant variability. In any case, the bulk-rock HREE composition of the A403 harzburgite suggests a relatively high degree of partial (fractional) melting (*c.* 13%), whereas the HREE and Ti contents of bulk rock and clinopyroxenes of the N304 spinel lherzolite are consistent with a lower degree (*c.* 9%) of fractional melting under spinel-facies conditions.

The liquids calculated in equilibrium with the clinopyroxene of the N304 spinel lherzolite ($D^{cpx/L}$ values from Hart & Dunn 1993) are LREE depleted (La_N/Yb_N *c.* 0.15; La_N *c.* 1.6), with Th_N/La_N *c.* 0.32. Similar compositions have been documented for olivine tholeiites related to the Iceland plume, which were generated by melting of a refractory mantle source (Hemond *et al.* 1993).

In contrast, the hypothetical melts in equilibrium with clinopyroxene from the A403 spinel harzburgite have convex-upward patterns with a maximum in the MREE region and La_N/Yb_N *c.* 1 with La_N *c.* 10. These patterns are strictly similar to the integrated fractional liquids produced by

10% fractional melting in the garnet field plus 10% in the spinel field of a fertile source (Johnson *et al.* 1990). The melts so produced must have a tholeiitic composition. This character is also confirmed by the very low Th_N/La_N ratio of clinopyroxene and its theoretical equilibrium liquid.

In conclusion, the data discussed above indicate that the Group 2 peridotites experienced refertilization processes under spinel-facies conditions as a result of the uprise of melts generated in deeper mantle levels having different fertility. Alternatively, if the melts percolating the Group 2 peridotites were genetically related, it might be considered that the melt in equilibrium with the clinopyroxene of the N304 spinel lherzolite derived from a primitive melt similar in composition to the hypothetical melts in equilibrium with clinopyroxene of the A403 spinel harzburgite via reaction with a strongly refractory ambient peridotite.

Nurali Group 3 peridotite. The relative enrichment in LREE–MREE, Nb, Ta, Th, U and Zr displayed by clinopyroxene and amphibole from the A404 spinel harzburgite argue in favour of pervasive percolation of melts or fluids with alkaline geochemical signatures. The bulk-rock and mineral compositions of this harzburgite are characterized by very low amounts of highly fusible major elements, such as Al, Ca and Ti, thus suggesting a high degree of partial melting and/or pyroxene (± spinel or garnet) dissolution during the injection of the alkaline component. Xu *et al.* (1998) and Vannucci *et al.* (2002) proposed that spinel harzburgite having similar clinopyroxene composition could form the lowermost part of a lithospheric mantle column extensively re-equilibrated with large volumes of ocean-island basalt (OIB) melts from a deeper source.

Inferences on the geodynamic setting of the Nurali and Mindyak peridotites

The Nurali and Mindyak lherzolites possess some critical mineralogical, petrographic and geochemical features, which are objectively anomalous for an abyssal peridotite lithosphere *sensu stricto*. The main distinctive features are: (1) the mostly fertile composition of the peridotites (lherzolitic rather than harzburgitic); (2) the nature of the internal zoning of the peridotite mode, which varies from lherzolite to dunite through harzburgite; (3) the presence of an anomalous crust–mantle transition zone, which includes amphibole-bearing, plagioclase-free ultramafic cumulates; (4) the lack of evidence of a crustal section related to the peridotites, and in particular of a gabbroic lower crust; (5) the intrusion of gabbro–diorite experienced by the upper part of the crust–mantle transition zone at about 400 Ma, that is, the time of closure of the Uralian Ocean by intra-oceanic subduction.

The petrographical and geochemical data presented in this paper show that the investigated peridotites of the Nurali and Mindyak massifs underwent multistage events of reactive porous-flow possibly accompanied, or preceded, by pyroxene dissolution and/or partial melting. On the other hand, the only melt percolation event that can be straightforwardly related to an oceanization process is the plagioclase crystallization, which is well documented in oceanic and transitional ocean–continent environments. In contrast, the lithological zoning recorded by the upper part of both massifs and their geochemical gradients are typical of subcontinental to continent–ocean transition mantle (Western Alps massifs, Zabargad, Lanzo) rather than of mantle sectors from a truly oceanic lithosphere.

Although largely speculative because of the limited sampling and the lack of isotope-based time constraints, two models (hereafter called Model 1 and Model 2) can be proposed to account for the anomalous (for abyssal peridotites) features of the Nurali and Mindyak massifs and to integrate the results of this geochemical study with the previous knowledge about these ultramafic massifs. In Model 1, the anomalous features were acquired after the oceanization process. Alternatively, in Model 2 they are considered to have preceded the plagioclase crystallization. Accordingly, these models offer alternative scenarios for the geological settings and the geodynamic evolution of the Nurali and Mindyak ultramafic massifs.

In Model 1, the sequence of events is tentatively reconstructed as follows.

(1) The Nurali and Mindyak peridotites belonged to a 'normal' oceanic lithosphere generated by mid-ocean ridge processes of the Uralian basin. These processes could be recorded in the spinel and spinel ± plagioclase peridotites of the Nurali ridge that show evidence of a moderate partial melting event (≤9%) associated with, or followed by, refertilization processes via melt percolation.

(2) Later, the upper part of the mantle ultramafic sequences experienced the percolation of large melt volumes, which generated the Nurali harzburgite–dunite zone and which are recorded by the Mindyak spinel lherzolite to spinel harzburgite transition. These magmatic events had tholeiitic to alkaline geochemical signatures and were related to intra-plate or, more likely, to island-arc magmatism. The dunite–wehrlite–pyroxenite transition zone of Nurali could be a result of these magmatic episodes rather than of mid-ocean ridge

processes. The lack of conduits or channels clearly connected to the magma percolation of the Nurali and Mindyak upper zones suggests that this zone was fed laterally.

(3) The final, pre-orogenic events recorded by the Nurali and Mindyak massifs are related to the subduction of the Uralian oceanic lithosphere and to the processes that occurred in sectors of the mantle wedge. During the subduction event dated at about 400 Ma the Moho sections of Nurali and Mindyak sequences were intruded by magmas that generated the gabbro–diorite sequence.

For Model 2, a more complicated series of events is considered.

(1) The Nurali and Mindyak peridotites were part of a subcontinental lithospheric mantle before the opening of the Uralian Ocean. The peridotites at this stage were probably variably depleted lherzolites that experienced deep-seated magmatism and sub-solidus re-equilibration.

(2) During the precursor phases of the extensional process related to the opening of the Uralian Ocean, sectors of the asthenospheric mantle underwent decompression partial melting and large volumes of melts migrated upward, interacting with the overlying peridotite lithospheric mantle. The melt–peridotite interaction was progressively more intense towards the mantle–crust transition, thus forming dominant harzburgite and dunite bodies upsection, essentially via pyroxene dissolution, and resulting in an underplating process. A similar process has been invoked to describe the intrusion of the Basic Complex of the Ivrea–Verbano Zone (Western Alps) related to the extensional regime preceding the opening of the Tethys Ocean during Jurassic time. At Nurali, this stage could be recorded by the recrystallization of the spinel lherzolite and spinel harzburgite. The geochemical signature of the rising melts was dominantly tholeiitic. The variation of the trace element composition of the spinel-facies clinopyroxene indicates that geochemical gradients developed during the melt percolation and/or the peridotites were intruded by variously fractionated melts.

(3) During the break-up of the continental lithosphere the mantle peridotites were partially intruded at shallower depth by tholeiitic melts. This event is marked by plagioclase crystallization; the absence of exsolution lamellae in the coexisting pyroxene formed by the percolating melt that produced plagioclase suggests that the massifs rapidly froze after this melt injection.

(4) The final events recorded by the Nurali and Mindyak massifs are closely related to subduction, as described in point (3) of Model 1.

In conclusion, Model 1 is an attempt to reconcile our petrographic and geochemical data with the common geodynamic interpretation of the Nurali and Mindyak sequences (namely, oceanic peridotite, possibly involved in island-arc processes). In this scenario, the occurrence of spinel ± plagioclase peridotites overlain by spinel peridotites depleted in fusible elements and with evidence of significant melt percolation suggests that these sequences were probably located in a transitional area between oceanic and sub-arc lithosphere. An alternative scenario is proposed by Model 2, which is aimed at providing new matter for debate on the interpretation of the trace element fingerprints of the southern Urals ultramafic bodies.

Important contributions to a more precise assessment of the geological setting and the geodynamic evolution might be furnished by further research aimed at characterizing geochemical gradients occurring in the Nurali harzburgite–dunite sequence and in the Mindyak spinel lherzolite to harzburgite transition. Such research would provide precious insights into the primitive composition of the percolating melts, the physico-chemical parameters ruling the melt–peridotite reactions and the sequence of the events.

We thank G. Savelieva for donation of Nurali samples. She, the unforgettable colleague and friend A. A. Saveliev and A. N. Pertsev have helped with fieldwork, exchange of ideas, suggestions, and useful discussions. We are grateful to F. Bea for producing high-quality trace element data. We thank R. Carampin for assistance during the microprobe chemical analyses of minerals in Padova, and M. Dini and J. H. Scarrow for help with chemical analyses of minerals. We thank Y. Dilek, E. Konstantinovskaya, S. Arai and an anonymous reviewer, who provided frank, constructive reviews. Financial support from the European Commission (TMR-URO Programme), the European Science Foundation (EUROPROBE Programme), and the Italian Ministry of Education, University and Scientific Research (Progetto Nazionale MURST-Cofin98) is acknowledged. The Italian National Research Council has made possible the microprobe work at the University of Padova.

References

ANDERS, E. & GREVESSE, N. 1989. Abundances of the elements: meteoric and solar. *Geochimica et Cosmochimica Acta*, **53**, 197–214.

ARAI, S. 1987. An estimation of the least depleted spinel peridotites on the basis of olivine–spinel mantle array. *Neues Jahrbuch für Mineralogie, Monatshefte*, 347–357.

BODINIER, J.-L., MENZIES, M.A. & THIRLWALL, M.F. 1991. Continental to oceanic mantle transition—REE and Sr–Nd isotopic geochemistry of the Lanzo lherzolite massif. *Journal of Petrology, Lherzolite Special Issue*, 191–210.

BONATTI, E. & MICHAEL, P.J. 1989. Mantle peridotites from continental rifts to ocean basins to subduction

zones. *Earth and Planetary Science Letters*, **91**, 297–311.

BONATTI, E., OTTONELLO, G. & HAMLYN, P.R. 1986. Peridotites from the Island of Zabargad (St. John), Red Sea: petrology and geochemistry. *Journal of Geophysical Research*, **91**, 599–631.

BONATTI, E., SEYLER, M. & SUSHEVSKAYA, N. 1993. A cold suboceanic mantle belt at the Earth's equator. *Science*, **261**, 315–320.

BREY, G.P. & KOHLER, T. 1990. Geothermobarometry in four-phase lherzolites II. New thermobarometers, and practical assessment of the existing thermobarometers. *Journal of Petrology*, **31**, 1353–1378.

BROWN, D. & SPADEA, P. 1999. Processes of forearc and accretionary complex formation during arc–continent collision in the southern Urals. *Geology*, **27**, 649–652.

BROWN, D., JUHLIN, C., ALVAREZ-MARRON, J., PEREZ-ESTAÙN, A. & OSLIANSKI, A. 1998. Crustal-scale structure and evolution of an arc–continent collision zone in the southern Urals, Russia. *Tectonics*, **17**, 158–171.

CHARPENTIER, S. 2000. *La zone de transition continent–océan de la marge continentale passive ouest-ibérique: études pétrologique et géochimique des roches magmatique and mantelliques*. PhD thesis, University Blaise Pascal, Clermont-Ferrand.

CIUFFI, S.I.A., ZANETTI, A., MAZZUCCHELLI, M., RIVALENTI, G. & CINGOLANI, C.A. 2001. The back-arc mantle lithosphere of the Andean volcanic front: xenoliths from Tres Lagos and Cerro Desconecido (Patagonia, Argentina). EUG 11, Strasbourg, France, 8–12 April. *Journal of Conference Abstracts*, **6**, 415.

CONREY, R.M., SHERROD, D.R., HOOPER, P.R. & SWANSON, D.A. 1997. Diverse primitive magmas in the Cascade arc, northern Oregon and southern Washington. *Canadian Mineralogist*, **35**, 367–396.

CORNEN, G., BESLIER, M.-O. & GIRARDEAU, J. 1996. Petrologic characteristics of the ultramafic rocks from the continent/ocean transition in the Iberia Abyssal Plain. *In:* WHITMARSH, R.B., SAWYER, D.S., KLAUS, A. & MASSON, D.G. (eds) *Proceedings of the Ocean Drilling Program, Scientific Results, 149*. Ocean Drilling Program, College Station, TX, 377–395.

CORTESOGNO, L., GAGGERO, L. & ZANETTI, A. 2000. Rare earth and trace elements in igneous and high-temperature metamorphic minerals of oceanic gabbros (MARK area, Mid-Atlantic Ridge). *Contributions to Mineralogy and Petrology*, **139**, 373–393.

DENISOVA, E.A. 1984. Internal structure of Mindyak ultramafic massif (Southern Urals). *Reports, Academy of Sciences*, **274**, 382–387 (in Russian).

FABRIÈS, J., BODINIER, J.-L., DUPUY, C., LORAND, J.-P. & BENKERROU, C. 1989. Evidence of modal metasomatism in the orogenic spinel lherzolite body from Caussou (Northeastern Pyrenees, France). *Journal of Petrology*, **30**, 199–228.

GAGGERO, L., SPADEA, P., CORTESOGNO, L., SAVELIEVA, G.N. & PERTSEV, A.N. 1997. Geochemical investigation of the igneous rocks from Nurali ophiolite mélange zone, Southern Urals. *Tectonophysics*, **276**, 139–161.

GARUTI, G., FERSHTATER, G., BEA, F., MONTERO, P., PUSHKAREV, E.V. & ZACCARINI, F. 1997. Platinum-group elements as petrological indicators in mafic–ultramafic complexes of the central and southern Urals: preliminary results. *Tectonophysics*, **276**, 181–194.

GASPARIK, T. 1984. Two-pyroxene thermobarometry with new experimental data in the system CaO–MgO–Al_2O_3–SiO_2. *Contributions to Mineralogy and Petrology*, **87**, 87–97.

GRUAU, G., GRIFFITHS, J.B. & LECUYER, C. 1998. The origin of U-shaped rare earth patterns in ophiolite peridotites: assessing the role of secondary alteration and melt/rock reaction. *Geochimica et Cosmochimica Acta*, **62**, 3545–3560.

HALLIDAY, A.N., LEE, D.-C., TOMMASINI, S., DAVIES, G.R., PASLIK, C.R., FITTON, J.G. & JAMES, D.E. 1995. Incompatible trace elements in OIB and MORB and source enrichment in the sub-oceanic mantle. *Earth and Planetary Science Letters*, **133**, 379–395.

HART, S.R. & DUNN, T. 1993. Experimental cpx/melt partitioning of 24 trace elements. *Contributions to Mineralogy and Petrology*, **113**, 1–8.

HEMOND, C., ARNDT, N.T., LICHTENSTEIN, U., HOFMANN, A.W., OSKARSSON, N. & STEINTHORSSON, S. 1993. The heterogeneous Iceland plume: Nd–Sr–O isotopes and trace element constraints. *Journal of Geophysical Research*, **98**, 15833–15850.

HETZEL, R., ECHTLER, H.P., SEIFERT, W., SCHULTE, B.A. & IVANOV, K.S. 1998. Subduction- and exhumation-related fabrics in the Paleozoic high-pressure/low-temperature Maksyutov Complex, Antingan area, southern Urals, Russia. *Geological Society of America Bulletin*, **110**, 916–930.

HOFMANN, A.W. 1988. Chemical differentiation of the Earth: the relationships between mantle, continental crust, and oceanic crust. *Earth and Planetary Science Letters*, **90**, 297–314.

IRVING, A.J. & FREY, F.A. 1984. Trace element abundances in megacrysts and their host basalts: constraints on partition coefficients and megacrysts genesis. *Geochimica et Cosmochimica Acta*, **48**, 1201–1221.

IVANOV, K.S., PUCHKOV, V.N. & BABENKO, V.A. 1990. Finds of conodonts and graptolites in metamorphic units of South Urals. *Doklady Academiya Nauk SSSR*, **310**, 676–679.

JOHNSON, K.T.M. & DICK, H.J.B. 1992. Open system melting and temporal and spatial variation of peridotite and basalts at the Atlantis II Fracture Zone. *Journal of Geophysical Research*, **97**(B6), 9219–9241.

JOHNSON, K.T.M., DICK, H.J.B. & SHIMIZU, N. 1990. Melting in the oceanic upper mantle: an ion microprobe study of diopsides in abyssal peridotites. *Journal of Geophysical Research*, **95**, 2661–2678.

KELEMEN, P.B., DICK, H.J.B. & QUICK, J.E. 1992. Formation of harzburgite by pervasive melt/rock reaction in the upper mantle. *Nature*, **358**, 635–641.

KELEMEN, P.B., SHIMIZU, N. & SALTERS, V.J.M. 1995. Extraction of mid-ocean-ridge basalt from the upwelling mantle by focused flow of melt in dunite channels. *Nature*, **375**, 747–753.

KINZLER, R.J. 1997. Melting of mantle peridotite at pressures approaching the spinel to garnet transition: application to mid-ocean ridge petrogenesis. *Journal of Geophysical Research*, **102**(B1), 853–874.

LAURORA, A., MAZZUCCHELLI, M., RIVALENTI, G., VANNUCCI, R., ZANETTI, A., BARBIERI, M.A. & CINGOLAMI, C.A. 2001. Metasomatism and melting in carbonated peridotite xenoliths from the mantle wedge; the Gobernador Gregores case (Southern Patagonia). *Journal of Petrology*, **42**, 69–87.

LENNYKH, V.I., VALIZER, P.M., BEANE, R. & ERNST, W.G. 1995. Petrotectonic evolution of the Maksyutov complex, Southern Urals, Russia: implications for ultrahigh-pressure metamorphism. *International Geology Review*, **37**, 584–600.

LUNDSTROM, C.C., SHAW, H.F., RYERSON, F.J., PHINNEY, D.L., GILL, J.B. & WILLIAMS, Q. 1994. Compositional controls on the partitioning of U, Th, Ba, Pb, Sr, and Zr between clinopyroxene and haplobasaltic melts: implications for uranium series disequilibria basalts. *Chemical Geology*, **128**, 407–423.

MATTE, PH., MALUSKI, H., GABY, R., NICHOLAS, A., KEPEZHINSKAS, P. & SOBOLEV, S. 1993. Geodynamic model and $^{39}Ar/^{40}Ar$ dating for generation and emplacement of high-pressure metamorphic rocks in SW Urals. *Comptes Réndus de l'Académie des Sciences, Série 2*, **317**, 1667–1674.

MAZZUCCHELLI, M., RIVALENTI, G., ZANETTI, A., VANNUCCI, R. & CAVAZZINI, G. 1999. Origin and significance of late noritic dykes in the Baldissero peridotite massif (Ivrea–Verbano Zone). *Ofioliti*, **24**, 129–130.

MCDONOUGH, W.F., STOSCH, H.G. & WARE, N.G. 1992. Distribution of titanium and rare earth elements between peridotitic minerals. *Contributions to Mineralogy and Petrology*, **110**, 321–328.

MELCHER, F., GRUM, W., THALHAMMER, T.V. & THALHAMMER, O.A.R. 1999. The giant chromite deposits of Kempirsai, Urals: constraints from trace elements (PGE, REE) and isotope data. *Mineralium Deposita*, **34**, 250–272.

PERTSEV, A.N., SPADEA, P., SAVELIEVA, G.N. & GAGGERO, L. 1997. Nature of the transition zone in the Nurali ophiolite, southern Urals. *Tectonophysics*, **276**, 163–180.

PICCARDO, G.B., MESSIGA, B. & VANNUCCI, R. 1988. The Zabargad peridotite–pyroxenite association: petrological constraints on its evolution. *Tectonophysics*, **150**, 135–162.

PICCARDO, G.B., RAMPONE, E., VANNUCCI, R., SHIMIZU, N., OTTOLINI, L. & BOTTAZZI, P. 1993. Mantle processes in the subcontinental lithosphere: the case study of the rifted sp-lherzolites from Zabargad (Red Sea). *European Journal of Mineralogy*, **5**, 1039–1056.

PICCARDO, G.B., RAMPONE, E., ZANETTI, A., ROMAIRONE, A. & BRUZZONE, S. 2002. Melt percolation and impregnation in the Lanzo South peridotite: preliminary field, petrographic and mineral chemistry results. *Annual Meeting of the Swiss Academy of Natural Sciences (SANW) 2002, 19–20 September, Davos (Switzerland), Abstracts*. 36–38.

PUCHKOV, V.N. 1997a. Structure and geodynamics of the Uralian orogen. *In:* BURG, J.-P. & FORD, M. (eds) *Orogeny through Time*. Geological Society, London, Special Publications, **121**, 201–236.

PUCHKOV, V.N. 1997b. Tectonics of the Urals: modern concepts. *Geotectonics*, **31**, 294–312.

RAFFONE, N., ZANETTI, A., CHAZOT, G., DENIEL, C. & VANNUCCI, R. 2001. Geochemistry of mantle xenoliths from Ibalrhatene (Mid Atlas, Morocco): insights into the lithospheric mantle evolution during continental rifting. *Eleventh Annual V. M. Goldschimdt Conference, May 20–24, Hot Springs, VA. Lunar and Planetary Institute Contribution*. **1088**, Abstract 3323.

RAMPONE, E., BOTTAZZI, P. & OTTOLINI, L. 1991. Complementary Ti and Zr anomalies in orthopyroxene and clinopyroxene from mantle peridotites. *Nature*, **354**, 518–521.

RAMPONE, E., PICCARDO, G.B., VANNUCCI, R., BOTTAZZI, P. & OTTOLINI, L. 1993. Subsolidus reactions monitored by trace element partitioning: the spinel- to plagioclase-facies transition in mantle peridotites. *Contributions to Mineralogy and Petrology*, **115**, 1–17.

RAMPONE, E., HOFMANN, A.W., PICCARDO, G.B., VANNUCCI, R., BOTTAZZI, P. & OTTOLINI, L. 1996. Trace element and isotope geochemistry of depleted peridotites from an N-MORB type ophiolite (Internal Ligurides, N. Italy). *Contributions to Mineralogy and Petrology*, **123**, 61–76.

RAMPONE, E., PICCARDO, G.B., VANNUCCI, R. & BOTTAZZI, P. 1997. Chemistry and origin of trapped melts in ophiolitic peridotites. *Geochimica et Cosmochimica Acta*, **61**, 4557–4569.

RIVALENTI, G., MAZZUCCHELLI, M., VANNUCCI, R., HOFMANN, A.W., OTTOLINI, L., BOTTAZZI, P. & OBERMILLER, W. 1995. The relationship between websterite and peridotite in the Balmuccia peridotite massif (NW Italy) as revealed by trace element variations in clinopyroxene. *Contributions to Mineralogy and Petrology*, **121**, 275–288.

SALTERS, V.J.M. & SHIMIZU, N. 1988. World-wide occurrences of HFSE-depleted mantle. *Geochimica et Cosmochimica. Acta*, **52**, 2177–2182.

SAVELIEV, A.A. & SAVELIEVA, G.N. 1991. The Kempersay ophiolite massif: main features of the structure and composition. *Geotectonika*, **6**, 57–65.

SAVELIEV, A.A., ASTRAKHANTSEV, O.V., KNIPPER, A.L., SHARASKIN, A.YA. & SAVELIEVA, G.N. 1998. Structure and deformation phases of the Northern Terminus of the Magnitogorsk Zone, Urals. *Geotectonika*, **3**, 38–50.

SAVELIEV, A.A., SHARASKIN, A.YA. & D'ORAZIO, M. 1999. Plutonic to volcanic rocks of the Voykar ophiolite massif (Polar Urals): structural and geochemical constraints on their origin. *Ofioliti*, **24**, 21–30.

SAVELIEV, A.A., BIBIKOVA, E.V., SAVELIEVA, G.N., SPADEA, P., PERTSEV, A.N., SCARROW, J.H. & KIRNOZOVA, T.I. 2001. Garnet pyroxenites of the Mindyak massif, South Urals: age and environment of their formation. *Bulletin MOIP*, **76**, 22–29 (in Russian).

SAVELIEVA, G.N. 1987. *Gabbro–Ultrabasite Assem-*

blages of Uralian Ophiolites and their Analogues in the Recent Oceanic Crust. Nauka, Moscow (in Russian).

SAVELIEVA, G.N. & NESBITT, R.W. 1996. A synthesis of the stratigraphic and tectonic setting of the Uralian ophiolites. *Journal of the Geological Society, London*, **153**, 525–537.

SAVELIEVA, G.N., SHARASKIN, A.YA., SAVELIEV, A.A., SPADEA, P. & GAGGERO, L. 1997. Ophiolites of the Southern Uralides adjacent to the East European continental margin. *Tectonophysics*, **276**, 117–137.

SAVELIEVA, G.N., SHARASKIN, A.YA., SAVELIEVA, A.A., SPADEA, P., PERTSEV, A.N. & BABARINA, I.I. 2002. Ophiolites and zoned mafic–ultramafic massifs of the Urals: a comparative analysis and some tectonic implications. *In:* BROWN, D., JUHLIN, C. & PUCHKOV, V. (eds) *Mountain Building in the Uralides: Pangea to the Present*. Geophysical Monograph, American Geophysical Union, **132**, 135–153.

SCARROW, J.H., SPADEA, P., CORTESOGNO, L., SAVELIEVA, G.N. & GAGGERO, L. 2000. Geochemistry of garnet metagabbros from the Mindyak ophiolite massif, Southern Uzals. *Ofioliti*, **25**, 103–115.

SEIFERT, K. & BRUNOTTE, D. 1996. Geochemistry of serpentinized mantle peridotite from Site 897 in the Iberia Abyssal Plain. *In:* WHITMARSH, R.B., SAWYER, D.S., KLAUS, A. & MASSON, D.G. (eds) *Proceedings of the Ocean Drilling Program, Scientific Results, 149*. Ocean Drilling Program, College Station, TX, 471–488.

SEITZ, H.-M., ALTHERR, R. & LUDWIG, T. 1999. Partitioning of transition elements between orthopyroxene and clinopyroxene in peridotitic and websteritic xenoliths: new empirical geothermometers. *Geochimica et Cosmochimica Acta*, **63**, 3967–3982.

SERAVKIN, I.B. 1997. Southern Urals: tectono-magmatic zoning and position among orogenic systems of the Uralo-Mongolian Belt. *Geotektonika*, **1**, 32–47 (in Russian).

SEYLER, M., TOPLIS, M.J., LORAND, J.-P., LUGUET, A. & CANNAT, M. 2001. Clinopyroxene microtextures reveal incompletely extracted melts in abyssal peridotites. *Geology*, **29**, 155–158.

SKULSKI, T., MINARIK, W. & WATSON, E.B. 1994. High-pressure experimental trace-element partitioning between clinopyroxene and basaltic melts. *Chemical Geology*, **117**, 127–147.

SMITH, I.E.M., WORTHINGTON, T.J., PRICE, R.C. & GAMBLE, J.A. 1997. Primitive magmas in arc-type volcanic associations: examples from the southwest Pacific. *Chemical Geology*, **35**, 257–273.

SPADEA, P. & SCARROW, J.H. 2000. Early Devonian boninites from the Magnitogorsk Arc, Southern Urals (Russia): implications for early development of a collisional orogen. *In:* DILEK, Y., MOORES, E., ELTHON, D. & NICOLAS, A. (eds) *Ophiolites and Oceanic Crust: New Insights from Field Studies and the Ocean Drilling Program*. Geological Society of America, Special Papers, **349**, 461–472.

SPADEA, P., KABANOVA, L.YA. & SCARROW, J.H. 1998. Petrology, geochemistry and geodynamic significance of Mid-Devonian boninitic rocks from the Baimak–Buribai area (Magnitogorsk Zone, Southern Urals). *Ofioliti*, **23**, 17–36.

SPADEA, P., D'ANTONIO, M., KOSAREV, A., GOROZHANINA, Y. & BROWN, D. 2002. Arc–continent collision in the Southern Urals: petrogenetic aspects of the forearc–arc complex. *In:* BROWN, D., JUHLIN, C. & PUCHKOV, V. (eds) *Mountain Building in the Uralides: Pangea to the Present*. Geophysical Monograph, American Geophysical Union, **132**, 101–134.

TIEPOLO, M., BOTTAZZI, P., PALENZONA, M. & VANNUCCI, R. 2003. A laser probe coupled with ICP-double focusing sector field mass spectrometer for in-situ analysis of trace elements in the geological samples and U–Pb dating of zircons. *Canadian Mineralogist*, **41**, 259–272.

VANNUCCI, R., PICCARDO, G.B. & RIVALENTI, G. *ET AL.* 1995. Origin of LREE-depleted amphiboles in subcontinental mantle. *Geochimica et Cosmochimica Acta*, **59**, 1763–1771.

VANNUCCI, R., ZANETTI, A., KEMPTON, P., CIUFFI, S., MAZZUCCHELLI, M. & CINGOLANI, C. 2002. The chemical history of young lithospheric mantle in a back-arc region: the spinel + garnet peridotite xenoliths from Pali Aike (South Patagonia). *In:* CINGOLANI, C.A. *ET AL.* (eds) *Acta del XV Congreso Geológico Argentino*. Asociation Geológica Argentina, Buenos Aires, Tomo III, 71–74.

WEBB, S.A.C. & WOOD, B.J. 1986. Spinel–pyroxene–garnet relationships and their dependence on Cr/Al ratio. *Contributions to Mineralogy and Petrology*, **92**, 471–480.

WELLS, P.R.A. 1977. Pyroxene thermometry in simple and complex systems. *Contributions to Mineralogy and Petrology*, **62**, 129–139.

WITT-EICKSCHEN, G. & SECK, H.A. 1991. Solubility of Ca and Al in orthopyroxene from spinel peridotite: an improved version of an empirical geothermometer. *Contributions to Mineralogy and Petrology*, **106**, 431–439.

XU, Y.-G., MENZIES, M.A., BODINIER, J.-L., BEDINI, R.M., VROON, P. & MERCIER, J.-C.C. 1998. Melt percolation and reaction atop a plume: evidence from the poikiloblastic peridotite xenoliths from Borée (Massif Central, France). *Contributions to Mineralogy and Petrology*, **132**, 65–84.

ZANETTI, A., VANNUCCI, R., OBERTI, R. & DOBOSI, G. 1995. Trace-element and crystal-chemistry of mantle amphiboles from the Carpatho-Pannonian Region. *Acta Vulcanologica*, **7**, 265–276.

ZANETTI, A., VANNUCCI, R., BOTTAZZI, P., OBERTI, R. & OTTOLINI, L. 1996. Infiltration metasomatism at Lherz as monitored by systematic ion-microprobe investigations close to a hydrous dike. *Chemical Geology*, **134**, 113–133.

ZANETTI, A., MAZZUCCHELLI, M., VANNUCCI, R. & RIVALENTI, G. 1999. The Finero phlogopite-peridotite massif: an example of subduction-related metasomatism. *Contributions to Mineralogy and Petrology*, **134**, 107–122.

ZONENSHAIN, L.P., KAZMIN, M.L. & NATAPOV, L.M. 1990. *Geology of the USSR: a Plate-Tectonic Synthesis*. American Geophysical Union, Geodynamics Series, **21**.